This manuscript has been submitted for publication in *Journal of Geophysical Research: Solid Earth.* Please note that, the manuscript is currently under peer review and has not been formally accepted for publication. Subsequent versions of this manuscript may have slightly different content.

The Effects of Characteristic Slip Distance on Earthquake Nucleation Styles in Fully Dynamic Seismic Cycle Simulations

Peng Zhai* and Yihe Huang#

Department of Earth and Environmental sciences
University of Michigan

*pengzhai@umich.edu
(PengZhai_UMich@twitter)

#yiheh@umich.edu

Jan 16, 2024

Abstract

Earthquake nucleation is a crucial preparation process of the following coseismic rupture propagation. Under the framework of rate-and-state friction (RSF), it was found that the ratios of a to b parameters control whether earthquakes nucleate as an expanding crack or a fixed length. However, the characteristic slip distance D_{RS} controls the weakening efficiency of fault strength and can influence the nucleation styles as well. Here we investigate the effects of D_{RS} on nucleation styles in the context of fully dynamic seismic cycles by evaluating the evolution of the nucleation zone quantitatively when it accelerates from the tectonic loading rate to seismic slip velocity. A larger a/b (>0.75) is needed to produce expanding crack nucleation styles for relatively small D_{RS}, which suggests that fixed length nucleation styles may dominate on natural and laboratory faults. Furthermore, we find that when the nucleation site is not in the center of the asperity, the constant weakening rate near 1 induces a more complex nucleation style. We also identify two special nucleation styles: one containing a temporary acceleration phase (foreshock-like) and the other including a failed acceleration phase (twin-like). We conclude that the earthquake nucleation style is strongly controlled by the value of D_{RS}. Future research needs to be cautious when selecting a few representative D_{RS} to study earthquake nucleation as well as foreshock activities. The possible dominance of fixed length nucleation styles also suggests that the minimum size of earthquake rupture may be estimated at the early stage of the nucleation phase.

Plain Language Summary

Understanding earthquake nucleation (i.e., how earthquakes start) is crucial for characterizing the source processes of earthquakes and mitigating the associated hazards. The rate-and-state dependent friction (RSF) law, which is derived from numerous laboratory rock friction experiments, has been applied to describe fault slip behavior quantitatively. It has been found that the ratio of a to b in RSF primarily controls the specific nucleation style, either an expanding crack or a fixed length patch. As another important parameter, D_{RS} controls the decreasing rate of fault friction and should also influence the nucleation style. Here, we explore the effects of D_{RS} on nucleation style in the context of earthquake cycles. We find that a larger a/b

(>0.75) is needed to produce the typical expanding crack nucleation style when D_{RS} is relatively small. For a wide range of a/b and D_{RS}, the fixed length nucleation style dominates. Our results reveal the critical role of D_{RS} on earthquake nucleation styles and suggest that the fixed length nucleation style may be more common on both natural and laboratory faults.

Key points

1. The characteristic slip distance controls the weakening efficiency of fault strength and influences the nucleation styles significantly.
2. Given a wide range of a/b and D_{RS}, fixed length nucleation styles are more common than expanding crack nucleation styles.
3. Nucleation sites can also affect the nucleation styles and two special nucleation styles have been recognized.

1. Introduction

Earthquakes are commonly considered as shear rupture instability on a pre-existing fault. Before the fast earthquake rupture propagation, a slow earthquake preparation process happens within an unstable region on the fault, or the so-called nucleation zone. Laboratory experiments (Latour et al., 2013; McLaskey, 2019; McLaskey and Kilgore, 2013; Ohnaka and Shen, 1999), theoretical analysis (Campillo and Ionescu, 1997; Uenishi and Rice, 2003), and numerical models (Ampuero and Rubin, 2008; Dieterich, 1992; Fang et al., 2010; Rubin and Ampuero, 2005) reveal that the nucleation zone accelerates continuously to a seismic slip velocity during the nucleation phase. Moreover, seismological observations validate the existence of the nucleation stage, which is associated with aseismic slip propagation and foreshock activities (Bouchon et al., 2013; Ellsworth and Beroza, 1995; Ide, 2019; McGuire et al., 2005; Tape et al., 2018). For example, Ellsworth and Beroza (1995) found that the size and duration of the nucleation phase is related to the eventual size of the earthquake. On the other hand, Ide (2019) found that the early parts of seismograms of different-sized earthquakes are highly similar, indicating that the ultimate size of the earthquake is difficult to predict using the nucleation phase.

The physical mechanisms responsible for earthquake nucleation can be better understood through numerical simulations, which provide a powerful tool to study earthquake processes in multiple scales of time and space. Earthquake cycle simulations based on the rate-and-state dependent friction (RSF) (Dieterich, 1979; Marone, 1998; Ruina, 1983) can model various earthquake phenomena comprising earthquake nucleation, foreshocks, coseismic rupture, aftershocks, postseismic afterslip, and interseismic aseismic transients (e.g., Barbot et al., 2012; Cattania and Segall 2021; Dieterich, 1992; Hetland and Simons, 2010; Hetland et al., 2010; Kaneko and Lapusta, 2008; Lapusta et al., 2000; Liu and Rice, 2005; Scholz, 1998; Tse and Rice, 1986). Essentially, the RSF allows us to understand the relationship between fault slip and empirical friction parameters derived from rock friction experiments. A standard form of the constitutive law is:

$$\frac{\tau}{\sigma_n} = \mu^* + aln\left(\frac{V}{V^*}\right) + bln\left(\frac{V^*\theta}{D_{RS}}\right) \quad (1)$$

Where τ is the frictional strength, σ_n is the normal stress, V is the sliding velocity, θ is the state variable indicating the real area of contact, μ^* and V^* are reference values of friction coefficient and slip velocity. The characteristic slip distance D_{RS} characterizes the evolution of θ and is the sliding distance required to reach a steady state following a perturbation in slip velocity. The parameter a represents the "direct effect": instantaneous fault friction changes with an abrupt (e-fold) velocity change. The parameter b describes the "evolution effect": variation of fault friction with the cumulative loading distance. Negative $a - b$ corresponds to steady state velocity-weakening (VW) friction and can result in dynamic instability within seismogenic zone, whereas positive $a - b$ corresponds to steady state velocity strengthening (VS) and is primarily responsible for aseismic slip.

The direct effect $aln\left(\frac{V}{V^*}\right)$ can arise from thermally activated creep processes at asperity contacts (e.g., Rice et al., 2001). Different from the direct effect, the evolution of state variable θ is usually empirical. In this study, we use the Dieterich's "aging" law (Dieterich, 1979), which considers the fault strengthens or heals with increasing stationary contact time:

$$\dot{\theta} = 1 - \frac{V\theta}{D_{RS}} \qquad \Omega = \frac{V\theta}{D_{RS}} \quad (2)$$

Where the dot denotes time derivatives. The $V\theta/D_{RS}$ term represents the weakening rate due to slip, which plays an important role in our study and is defined as Ω for simplicity.

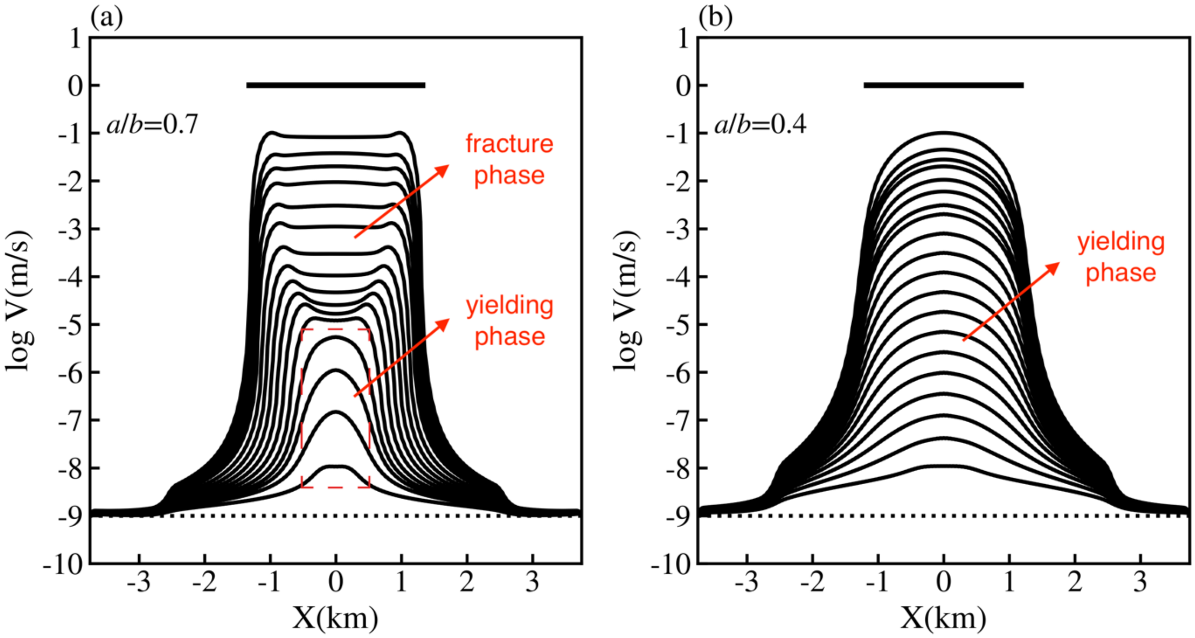

Fig. 1 Two representative nucleation styles: **(a)** expanding crack (yielding phase and fracture phase) and **(b)** fixed-length patch (only yielding phase). Horizontal bars in panel (a) and (b) represent $2L_\infty = 2\pi^{-1}[b/(b-a)]^2 L_b$ and $2* 1.3774 L_b$ respectively, where $L_b = \frac{GD_{RS}}{b\sigma_n}$. The dotted line represents background plate loading rate ($V_{pl} = 10^{-9}$ m/s).

There is a long history of studies about the earthquake nucleation length based on the RSF. First, a critical stiffness for instability with a spring-slider model has been derived as $k = (b-a)\sigma_n/D_{RS}$, which implies the critical nucleation length is proportional to $GD_{RS}/(b-a)\sigma_n$, where G is the generalized shear modulus (Rice, 1993; Ruina, 1983). When slip velocity is very high and the healing mechanism can be neglected, Dieterich (1992) suggested that the critical nucleation length should be proportional to b^{-1} instead of $(a-b)^{-1}$ and it equals $1.67 GD_{RS}/b\sigma_n$. Later, Rubin and Ampuero (2005) investigated the effects of a and b thoroughly and found that the ratio a/b controls the nucleation regime transition on rate and state faults governed by "aging" law, resulting in two different nucleation styles. When a/b > 0.5, nucleation consists of two phases: yielding phase and fracture phase. In the first yielding phase, frictional strength decreases with slip continuously and the nucleation zone keeps accelerating locally. While in the second fracture phase, fault strength remains nearly constant with slip and the nucleation zone keeps expanding with the half-length approaching $\pi^{-1}[b/(b-a)]^2$ $(GD_{RS}/b\sigma_n)$ (**Fig. 1a**). In contrast, if a/b is small enough (no-healing limit regime), the yielding phase dominates the whole nucleation phase with Ω>>1 (the state variable is rapidly decreasing) and the nucleation zone contracts to be a fixed length patch (**Fig. 1b**). Under this condition, the acceleration process within the nucleation zone remains localized until the consequent dynamic rupture propagation.

To clarify these scaling relationships, three characteristic lengths are defined:

$$L_b = \frac{GD_{RS}}{b\sigma_n} \quad L_{b-a} = \frac{GD_{RS}}{(b-a)\sigma_n} = \frac{b}{b-a}L_b \quad L_\infty = \frac{L_b}{\pi(1-a/b)^2} \tag{3}$$

Which are the same as the notations defined by Rubin and Ampuero (2005). But the actual critical length of the nucleation zone also involves other factors. For example, the factor 1.67 associated with the critical nucleation length discovered by Dieterich (1992) is dependent on slip and stress conditions along the fault.

It is worth noting that though the critical nucleation length estimated by Dieterich (1992) scales with L_b and results from a fixed length patch, a/b used in that study ranges from 0.625 to 0.888, which falls in the range of a/b that produces an expanding crack nucleation style in the models shown by Rubin and Ampuero (2005). However, Rubin and Ampuero (2005) also mentioned that the nucleation zone may scale with L_b when a/b > 0.5 if the weakening rate Ω is sufficiently large at the final stage of nucleation. This implies that the nucleation style is influenced by both a/b and the specific evolution of Ω, and these two studies can be reconciled when the effects of weakening rate are considered (Fang et al., 2010). For the “aging” version of the evolution law, it is the characteristic slip distance D_{RS} that controls the weakening rate of fault friction, which implies that the nucleation style is strongly affected by the D_{RS}.

Under the framework of RSF with the “aging” law, we conduct 2-D anti-plane fully dynamic seismic cycle simulations to unveil the prominent effects of D_{RS} on nucleation styles in the context of seismic cycles. We find that as D_{RS} decreases, larger a/b is necessary for the occurrence of expanding crack nucleation style. For a wide range of a/b and D_{RS}, the fixed length nucleation is dominant. We also find that the nucleation site affects nucleation styles. The typical expanding crack nucleation style only occurs when earthquakes nucleate in the center of the asperity and rupture bilaterally. Moreover, we recognize two special nucleation styles: one nucleation style containing a temporary acceleration phase ahead of the following expanding phase (foreshock-like) and the other including a failed acceleration phase, which initiates at the same time with the successful one (twin-like).

2. Model Setup

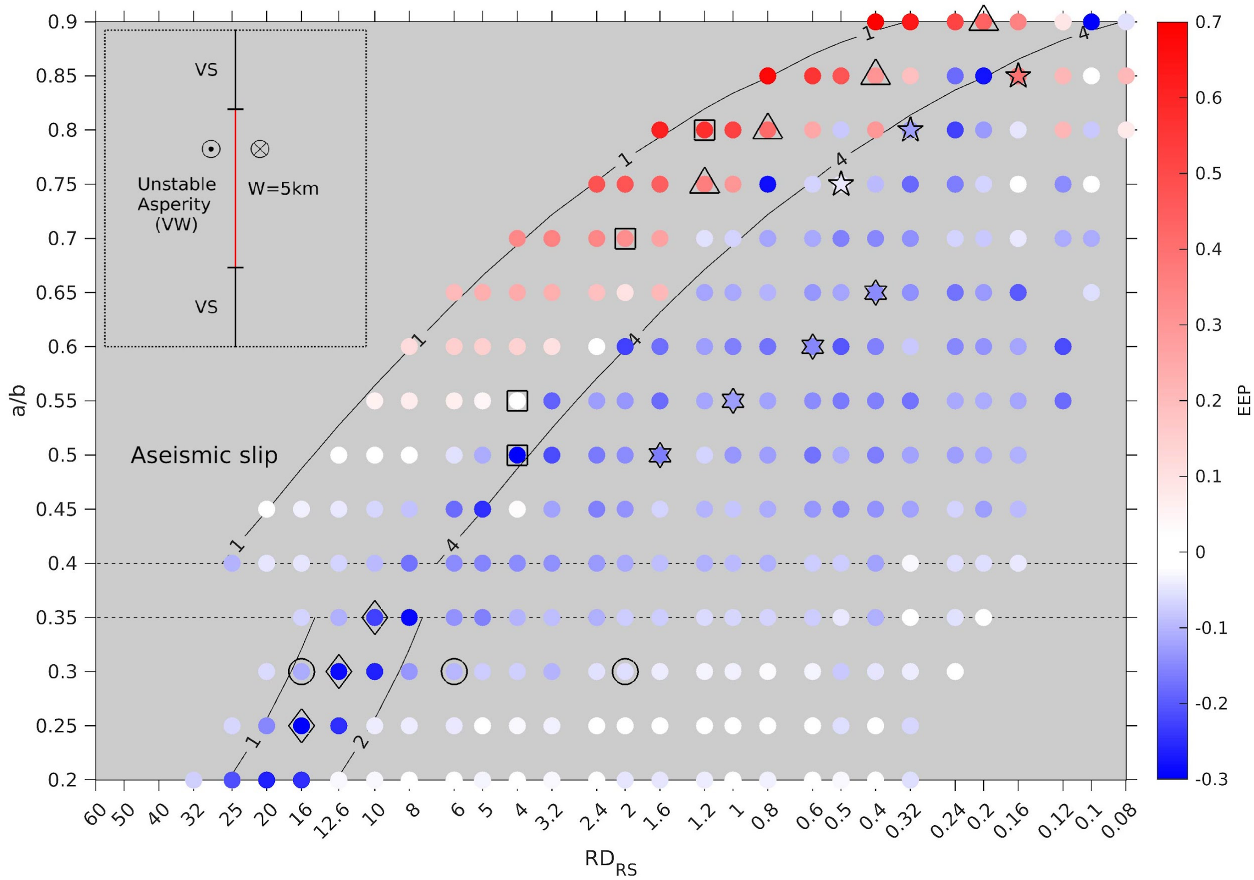

Fig. 2 Model setup(inset) and average EEP values under variable normalized characteristic weakening distance RD_{RS} ($10^6 \times \frac{D_{RS}}{W}$) and a/b ratio. The two black contours mean the ratio of asperity size (5 km) to the theoretical critical nucleation length (two different equations are applied) equals 1 and 4 (or 2 for a/b<0.3781), respectively. Red and blue dots represent cases with positive EEP and negative EEP values, respectively. Different black symbols denote simulations with different representative nucleation styles, which will be displayed and analyzed in detail later.

Table 1. Model parameters

Frictional properties (within asperity)	Symbol	Value
Static friction coefficient	μ^*	0.6
Reference slip velocity	V^*	10^{-6} m/s
Plate loading rate	V_{pl}	10^{-9} m/s
Direct effect (constant)	a	0.015
Ratio of a to b	a/b	0.2-0.9
Characteristic slip distance	D_{RS}	0.4-300 mm
Physical properties		
Effective normal stress	σ_n	40 MPa
Asperity size	W	5 km
Shear wave speed	C_s	3462 m/s
Shear modulus of host rock	G	32 GPa
Nucleation threshold	V_{dyn}	0.1 m/s

We consider a two-dimensional anti-plane shear model where the displacement is out of the plane of interest (inset of **Fig. 2**). Our model is elastic and homogeneous, and no off-fault heterogeneity is considered in this study. We simulate fully dynamic earthquake cycles using the spectral element method (Kaneko et al., 2011; Thakur et al., 2020). The length of the fault is 10 km and the distance between the lateral boundary and the fault is 8 km. Domain size tests show that nucleation styles are not influenced by a larger model domain. The fault is governed by the RSF friction ("aging" law) while all the other three boundaries are absorbing boundaries. The asperity (VW) is in the center of the fault with a width of 5 km. We also set up two strong barriers (VS) aside the VW asperity respectively to hinder the outward penetration of coseismic rupture. The distributions of a and b are symmetric with respect to the middle of the fault. All key parameters are summarized in **Table 1**.

To avoid the singularity when slip velocity approaches zero in expression (1), we utilize the regularized form of RSF in our seismic cycle simulations (Ben-Zion and Rice, 1997; Lapusta et al., 2000; Rice and Ben-Zion, 1996):

$$\tau = a\sigma_n arcsinh\, [\frac{V}{2V^*} exp\, (\frac{\mu^* + bln(V^*\theta/D_{RS})}{a})] \quad (4)$$

The quasi-static process zone at rupture speed 0^+ is defined as:

$$\Lambda_0 = \frac{9\pi}{32} L_b \quad (5)$$

For all the models presented here, the process zone includes at least 3 GLL nodes, which meets the criterion of ensuring numerical convergence (Day et al., 2005).

The rupture style and recurrence pattern of seismic cycles are also controlled by the ratio of the asperity size to critical nucleation length (Barbot, 2019; Cattania, 2019; Kato, 2004; Liu and Rice, 2007; Nie and Barbot, 2022; Rubin, 2008; Werner and Rubin, 2013; Wu and Chen, 2014). For example, Barbot (2019) proposed that Ru number (Dieterich-Ruina-Rice number) controls the rupture style and recurrence pattern at first order. The Ru number defines the ratio of the asperity size to the critical nucleation length estimated from the linear stability analysis (LSA), which is scaled with L_{b-a} (Rice, 1993; Ruina, 1983). However, this criterion is only valid for the no-healing limit regime when L_{b-a} can be approximated by L_b. When the fracture phase (i.e., constant weakening regime) dominates the final stage of nucleation, an energy criterion should be applied to estimate the upper limit of the critical nucleation length (Rubin and Ampuero, 2005).

For this reason, we choose the equations from Rubin and Ampuero (2005) to estimate the critical nucleation length in seismic cycles. The ratio of the asperity size (W) to the critical nucleation length (h^*) is defined as RA number:

$$RA = \frac{W}{h^*} \tag{6}$$

Where $h^* = 2L_\infty$ when $a/b > 0.5$ and $h^* = 2 * 1.3774L_b$ when $a/b < 0.3781$. The first h^* is derived based on an energy-based approach for fracture phase and the second one is applicable when the yielding phase dominates, and fault healing is not important.

Compared with the Ru number, the RA number is expected to work better in predicting rupture styles because of a more accurate estimation of h^* under the framework of aging law. It should be noted here, even though $h^* = 2L_\infty$ only works well for $a/b > 0.5$ as suggested by Rubin and Ampuero (2005), we still use this equation to estimate the critical nucleation length when $0.3781 <= a/b <= 0.5$ as other equations are not available for this range of a/b.

We examine nucleation styles in fully dynamic seismic cycles with two parameters of interest: a/b and D_{RS}. The ratio of a to b controls the relative contribution of direct effect and evolution effect in RSF friction while D_{RS} determines the weakening rate (Ω) of fault friction due to slip. The frictional properties significantly depend on the rock type. For example, Reinen et al. (1992) suggested that a/b could be as low as 0.1 for antigorite at room temperature, whereas a more widely accepted model derived from experiments on granite indicates that a/b can be as large as 0.9 (Blanpied et al., 1998). On the other hand, environmental factors, such as temperature and presence of water can also influence the value of a/b (Marone, 1998). For many laboratory experiments, only $a - b$ is reported while a/b is usually omitted, which further increases the difficulty to find a reasonable range of a/b. In this study, a/b varies from 0.2 to 0.9 with an interval of 0.05. There also exists a large uncertainty in the estimation of the characteristic slip distance D_{RS} whose scale-dependence is still debated. D_{RS} inferred from laboratory experiments is usually smaller than 0.1 mm (Dieterich, 2007). However, D_{RS} estimated from geophysical observations on large natural faults can be as high as a fraction of meter. For example, Guatteri et al. (2001) inferred that D_{RS} is 0.01-0.05 m for the fault hosting the 1995 Kobe earthquake. Moreover, the D_c'' (defined as an approximation of the slip-weakening distance D_c on strike-slip faults) is estimated to be within a range of 0.1-4.9 m for major earthquakes (compiled by Chen et al. (2021). As suggested by Cocco and Bizzarri (2002), D_c can be approximately related to D_{RS} by $\frac{D_c}{D_{RS}} = 15$. Therefore, the corresponding D_{RS} for major earthquakes is roughly 0.06-0.33 m, which is about 3 magnitudes larger than the laboratory inferred values. In this study, we explore a wide range of D_{RS} between 0.4 mm and 300 mm for a 5 km long fault. The lowest D_{RS} used in our study is close to the upper limit of estimated values from laboratory earthquakes. To eliminate the possible effects of scale-dependence, D_{RS} is normalized by the asperity size(W) and the ratio RD_{RS} is defined as $10^6 \times \frac{D_{RS}}{W}$.

3. Quantitative evaluation of nucleation styles

As mentioned previously, there exist two end-member nucleation regimes. Constant weakening regime depends on relatively large a/b as well as the initial state and loading conditions (Fang et al., 2010; Kaneko and Lapusta, 2008; Rubin and Ampuero, 2005), while the fixed length solution occurs in the no-healing limit regime with sufficiently small a/b (Rubin and Ampuero, 2005). When a/b is large, the nucleation phase includes an early localized yielding phase and a second expanding fracture phase controlled by the constant weakening regime. When a/b is small, the no-healing limit regime results in only the yielding phase.

Both kinds of nucleation styles have an early localized yielding phase with an increasing Ω and it is the further evolution of Ω that determines the ultimate nucleation regime. If Ω increases monotonously to a large value, the no-healing limit regime will lead to a fixed length nucleation. If Ω increases at first but then decreases to a constant value near 1, the constant weakening regime will lead to an expanding crack nucleation.

Even though the fixed length patch and expanding crack nucleation style appear to have different spatial and temporal distribution of slip velocity, how to distinguish them quantitatively remains an outstanding question. During each nucleation phase, the nucleation zone accelerates from a slow background loading rate (~10^{-9} m/s) to a fast seismic slip velocity (~1 m/s). Therefore, it is necessary to measure the length of the nucleation zone consistently until the dynamic instability is reached. In this study, we use the distribution of slip velocity to image the details of the nucleation stage.

We first define a slip velocity threshold (V_{dyn}), which indicates the end of the nucleation phase as well as the beginning of dynamic instability. When the peak slip velocity (V_{max}) reaches this threshold, the inertial effect starts to be significant. Based on the analysis of one-dimensional spring-block slider cycles (Rubin and Ampuero, 2005)

$$V_{dyn} = 2C_s a\sigma_n/G,\ \Omega \gg 1\ ;\ \ V_{dyn} = 2C_s(a-b)\sigma_n/G,\ \Omega = const. \tag{7}$$

Where C_s is shear wave speed. For simplicity, it is considered that $\Omega \gg 1$ corresponds to $\frac{a}{b} < 0.3781$ while $\Omega = const.$ corresponds to $\frac{a}{b} > 0.3781$. With the selected parameters in **Table 1**, the range of V_{dyn} is between 0.014 m/s and 0.195 m/s. Hence, we define 0.1 m/s as the nucleation threshold in this study.

To describe the expansion or contraction of each nucleation phase quantitatively, we define another parameter, called expanding efficiency parameter (EEP):

$$EEP = \sum_{i=2}^{7} \frac{log_{\ 10}(L_i) - log_{10}\ (L_{i-1})}{log_{10}(Vmax_i) - log_{10}(Vmax_{i-1})} \tag{8}$$

Where L_i is the measured width of slip velocity envelope with the corresponding peak slip velocity $Vmax_i$. To calculate EEP, we measure the nucleation length at 7 different peak slip velocities $Vmax_i$ that range from 10^{-7} m/s to 10^{-1} m/s, with the subsequent peak slip velocity threshold one magnitude larger than the previous one. The nucleation length is measured using the width of the spatial distribution of slip velocity that is larger than a threshold of 0.1*$Vmax_i$. We obtain 7 measurements of $L_i(\ i = 1{\sim}7)$ for each nucleation phase, which reflects the evolution of nucleation zone length. We then calculate EEP as the discrete derivative of the L_i with respect to $Vmax_i$ in the log domain, which represents either expansion or contraction of the nucleation zone. Positive EEP means that the expanding effect is dominant during earthquake nucleation (i.e., expanding crack nucleation), while negative EEP suggests the contracting effect is more significant (i.e., fixed length nucleation).

4. Results

4.1 Phase diagram of EEP

In this study, we only analyze the nucleation style of regular seismic events with peak slip velocity exceeding V_{dyn} (i.e., 0.1 m/s). Nearly all seismic events occur with a RA number larger than 1, which agrees with the principal idea that the critical nucleation length is supposed to be smaller than the asperity size for the generation of regular earthquakes, or otherwise aseismic slip (i.e., slow slip events, waves of partial coupling, and creep) will occur within the asperity. However, for some cases with small a/b (<0.3781), regular seismic events still happen when RA<1, partially because a certain amount of slip penetrates the barriers on the boundary and the peak slip velocity can still exceed the nucleation threshold. These abnormal seismic events can be mitigated by setting stronger velocity-strengthening regions, and they are not considered in the evaluation of nucleation styles.

For all qualified cases, 5 earthquakes after the spin-up time are chosen to calculate the EEP values. In the same seismic cycle, earthquakes can be either large or small in magnitude, but they nearly have the same critical nucleation length as well as nucleation styles. Hence, the choice of representative seismic events has a minimal influence on the calculation of EEP. We also use the average of the 5 EEP measurements to quantitatively evaluate the nucleation style for that simulation.

We find most cases have negative or near zero EEP values (blue or white dots in **Fig. 2**) while only a small portion have positive EEP values (red dots in **Fig. 2**). It is obvious that all cases with significant expanding effects have a/b over 0.5, which is consistent with the results of Rubin and Ampuero (2005). In addition, the nucleation style is affected by RD_{RS} substantially. With a relatively small RD_{RS}, a larger a/b (>0.5) is required for a positive EEP value (i.e., significant expanding effects). For example, when RD_{RS} is around 0.2, a/b must be larger than 0.75 to produce expanding crack nucleation.

One interesting phenomenon is that nearly all cases with significant expanding effects are bounded by RA contours of 1 and 4, respectively. As stated before, RA=1 ensures that regular earthquakes can occur, while RA=4 delineates the transition between bilateral ruptures (earthquakes nucleated in the center of the asperity) and unilateral ruptures (earthquakes nucleated at either one side of the asperity). This implies that nucleation styles can also be influenced by the specific rupture style (or the nucleation site of earthquakes), which is discussed further in section 5.2.

4.2 Different nucleation styles and the corresponding evolution of Ω

We recognize different nucleation styles in our simulations and discuss their main characteristics in this section. We first present simulations associated with $a/b > 0.3781$ and bilateral ruptures (black squares in **Fig. 2**). With increasing a/b and decreasing RD_{RS}, the nucleation style gradually changes from a fixed length to an expanding crack. In addition, we also discuss four examples with a temporary acceleration phase (black triangles in **Fig. 2**). We then focus on four cases with unilateral ruptures and negative EEP values, which produce fixed length nucleation with a/b>0.5 (black hexagons in **Fig. 2**). We also identify three special cases with unilateral ruptures and constant weakening regime (black pentagrams in **Fig. 2**). Their nucleation styles appear to be more complex than typical expanding crack nucleation.

We discuss simulations associated with $a/b < 0.3781$ as well. Typically, the fixed length nucleation always occurs with a monotonously increasing weakening rate (black circles in **Fig. 2**). A few cases (twin-like nucleation style) have very small EEP (black diamonds in **Fig. 2**) and they center around the contour line of RA=2 (or RA=4 for a/b>0.3781).

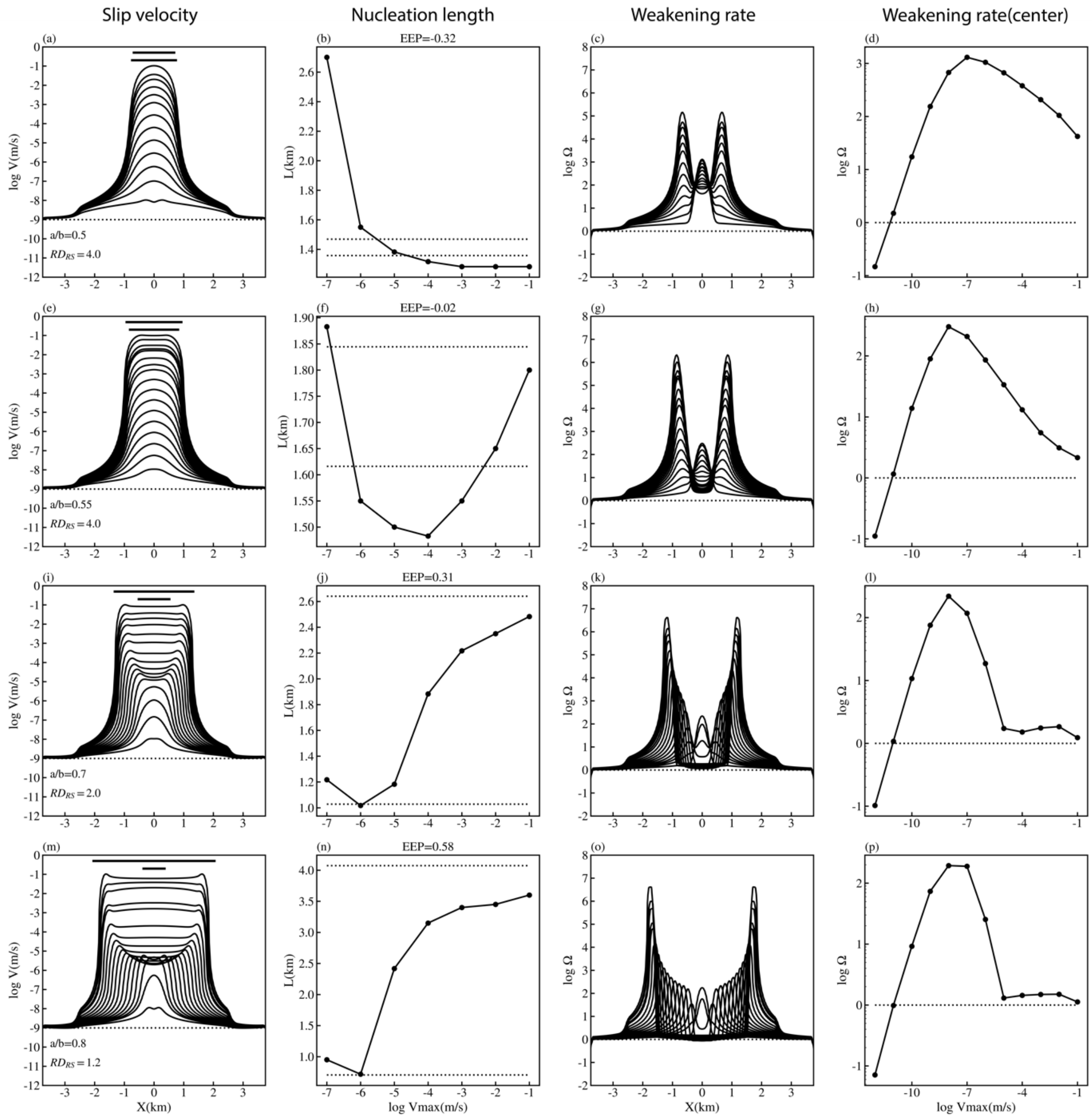

Fig. 3. Spatial and temporal evolution of slip velocity (first column), nucleation length measured at different slip velocities and the associated EEP value (second column), spatial-temporal evolution of Ω (third column), and Ω in the center of the nucleation zone as a function of peak slip velocity (fourth column). Four representative examples (dots surrounded by black squares in **Fig. 2**) with bilateral ruptures are displayed. In the first column, the top and bottom horizontal bars represent $2L_\infty$ and $2 * 1.3774L_b$, respectively, which correspond to two dotted lines in the second column. The dotted line in the first column is the background plate loading rate ($V_{pl} = 10^{-9}$ m/s). The dotted line in the third and fourth column represents the constant weakening rate (Ω=1).

4.2.1 a/b>0.3781 with bilateral ruptures

We present the evolution of V (slip velocity), EEP (expanding efficiency parameter), and Ω (weakening rate) of four cases with bilateral ruptures (black squares in Figure 1) in **Fig. 3**. All four cases have $a/b > 0.5$ but present distinct nucleation styles with increasing a/b and decreasing RD_{RS}. From top to bottom, the calculated EEP value increases from -0.32 to 0.58, signifying the transition of nucleation styles from a fixed length to an expanding crack.

For the typical fixed length nucleation associated with a negative EEP value of -0.32 (**Fig.2a-2d**), the nucleation zone contracts rapidly from 2.7 km to a fixed length of 1.3 km. Ω in the center of the nucleation zone increases at first and then decreases to a large value of ~100. In the second case that leads to almost zero EEP (**Fig. 3e-3h)**, the nucleation zone contracts initially but then begins to expand when the peak slip velocity exceeds 10^{-4} m/s. Like the first case, Ω in the center of the nucleation zone exhibits an initial increase and then decrease, approaching to a value of ~3. In the third case that results in a positive EEP of 0.31 (**Fig. 3i-3l)**, the nucleation zone starts to expand to the critical nucleation length when peak slip velocity exceeds 10^{-6} m/s. Ω in the center of the nucleation zone approaches a constant value of ~1 in the end, which is typical for the expanding nucleation style. Increasing a/b further leads to a larger EEP of about 0.6 (**Fig. 3m-3p**).

For the first example when a/b is close to 0.5, the estimated nucleation lengths from equations of L_b and L_∞ are nearly equivalent (lengths of two black bars in **Fig. 3a, 3e**). But when a/b becomes larger, even though the length of the initial yielding phase is still scaled by L_b, the critical nucleation length should be estimated as $2L_\infty$ for the fracture phase. We also notice there is temporary acceleration (**Fig. 3m**) at the transition from the localized yielding phase to the expanding fracture phase.

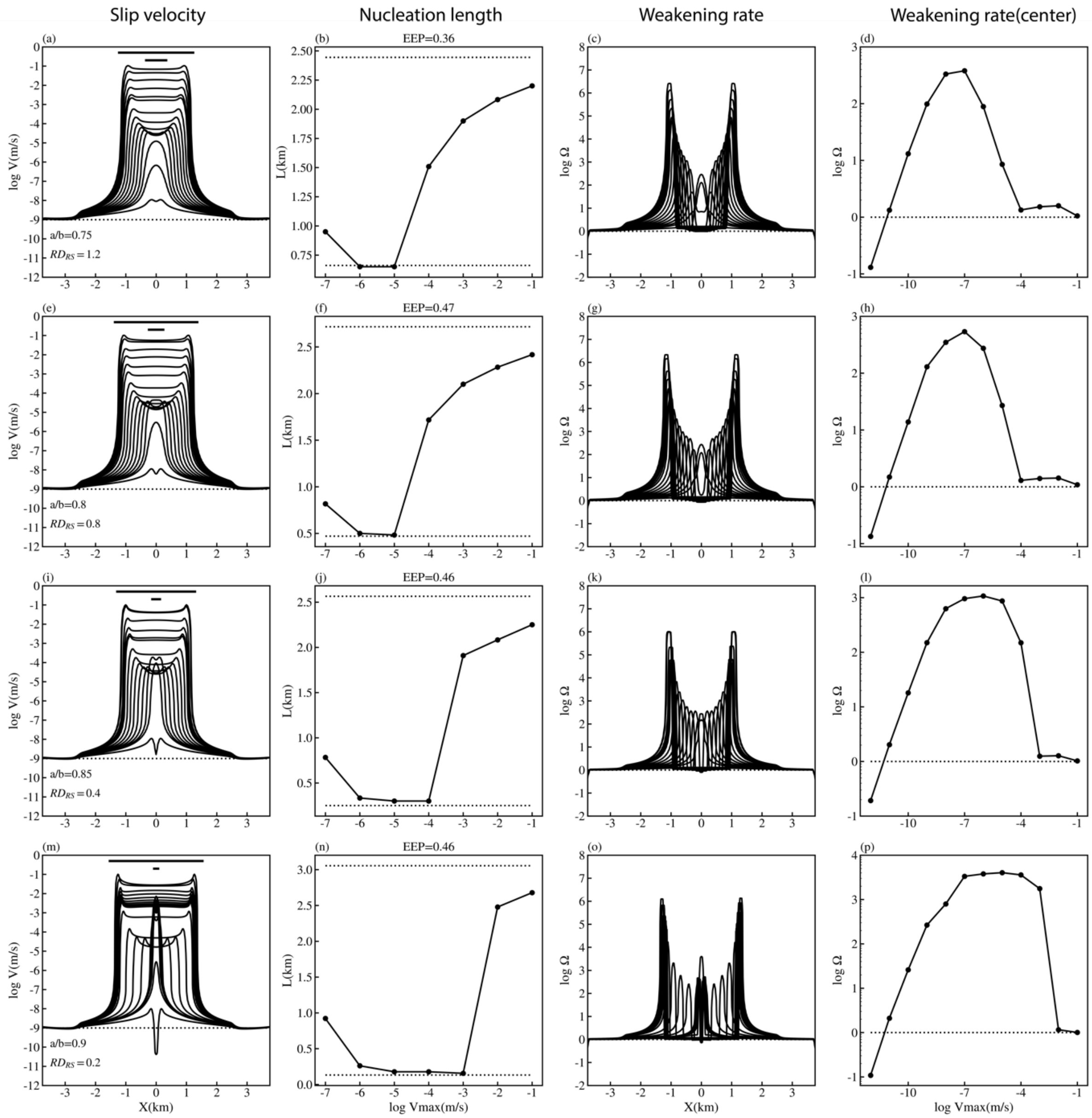

Fig. 4. Slip velocity (first column), measured nucleation length (second column), Ω (third column), and Ω in the center of the nucleation zone (fourth column) of four representative examples with bilateral ruptures, which are shown as dots surrounded by black up-pointing triangles in **Fig. 2,** respectively. In the first column, the top and bottom horizontal bars represent $2L_{\infty}$ and $2 * 1.3774L_b$, respectively, which correspond to two dotted lines in the second column. The dotted line in the first column is the background plate loading rate ($V_{pl} = 10^{-9}$ m/s). The dotted line in the third and fourth column refers to the constant weakening rate (Ω=1).

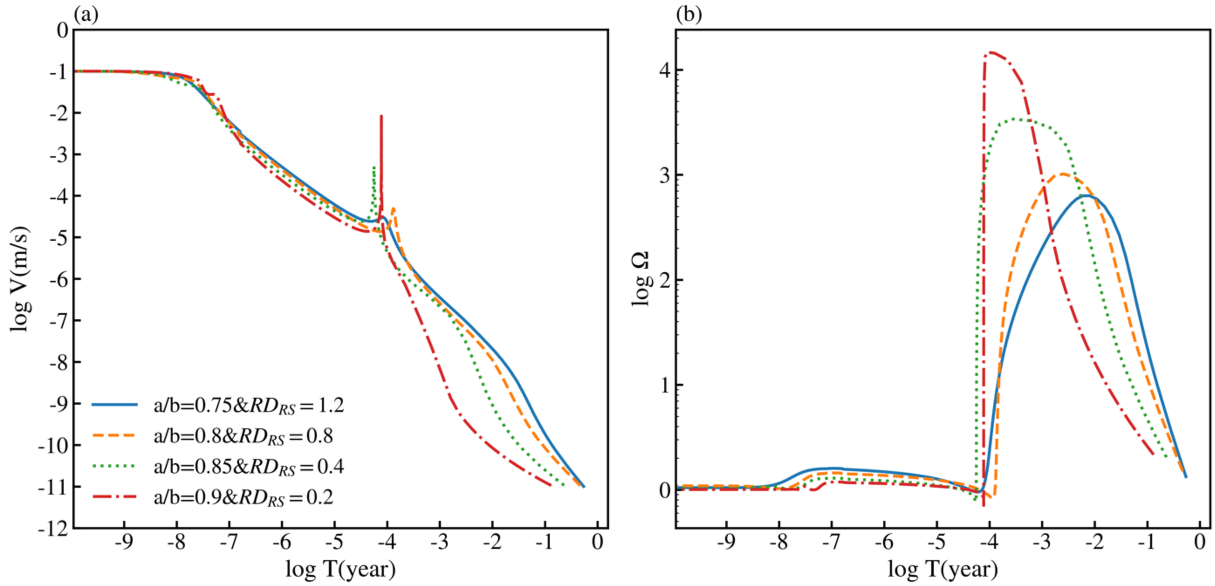

Fig. 5. Slip velocity (**a**) and Ω (**b**) in the middle of the nucleation zone as a function of T (time to instability).

We find that a temporary acceleration phase (foreshock-like) exists in some cases with a/b>=0.75 (**Fig. 4**). When a/b=0.9, the slip velocity even reaches a high value close to the nucleation threshold (0.1 m/s) at the end of the first yielding phase (**Fig. 4m**). After a slow-down process when Ω decreases to 1, the nucleation zone continues to accelerate and expand like a crack. However, the temporal evolution of nucleation lengths cannot capture this secondary acceleration phase well and only exhibits an abrupt variation (**Fig. 4j and 4n**). We also plot the temporal evolution of V and Ω in the center of the nucleation zone to describe the temporary acceleration phase in more detail (**Fig. 5**). The peak slip velocity occurs when the time to instability is about 10^{-4} year (< 1 day). The temporary acceleration of the first yielding phase is faster and accompanied with a more sharply variation of Ω (**Fig. 5b**). Ω decreases to ~1 at the onset of the secondary acceleration (i.e., fracture phase).

The occurrence of the temporary acceleration phase reveals that slip velocity does not have to increase monotonously during earthquake nucleation, and a secondary acceleration phase dominates the ultimate nucleation for sufficiently large a/b. This unstable transition from the yielding phase to fracture phase may be applied to explain some foreshock activities as suggested by Castellano et al. (2023). When a/b is as large as 0.9 (**Fig. 4m**), the length of the temporary acceleration phase is nearly one order of magnitude smaller than the critical nucleation length. Our results provide another possible explanation to the observed tiny source radii of foreshocks on laboratory faults [*McLaskey and Kilgore*, 2013] without introducing extra local stressing rate heterogeneity.

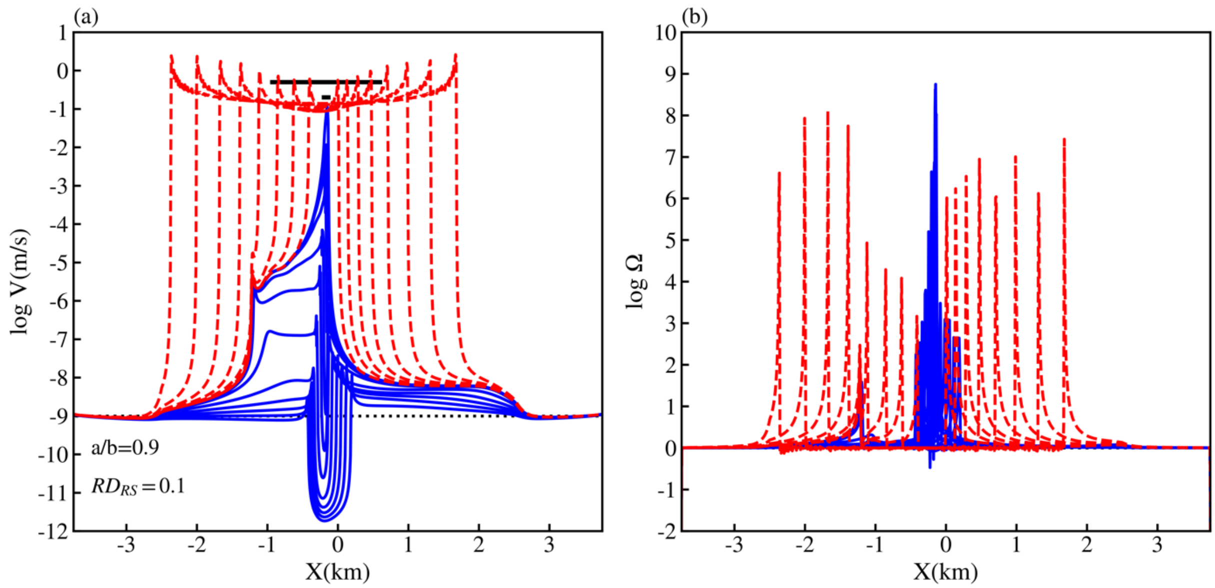

Fig. 6 Slip velocity (a) and Ω (b) during the nucleation phase (blue solid line) and rupture propagation (red dash line). The black dotted lines in panel (a) and panel (b) are background plate loading rate ($V_{pl} = 10^{-9}$ m/s) and constant weakening rate (Ω=1), respectively.

One special situation (a/b=0.9 and RD_{RS}=0.1) is that the yielding phase can trigger rupture propagation without a following fracture phase. In this case, the nucleation zone features an asymmetric acceleration, where an obvious fracture phase initiates at the early stage of nucleation (**Fig. 6**). Subsequently, the central region of the nucleation zone keeps accelerating and evolves into a small-scale yielding phase scaled with L_b instead of L_∞. This is in line with the previous results by Rubin and Ampuero (2005) (**Fig. 11b in their paper**), in which the yielding phase determines the critical nucleation length with a sufficiently large Ω.

4.2.2 a/b>0.3781 with other complex rupture styles

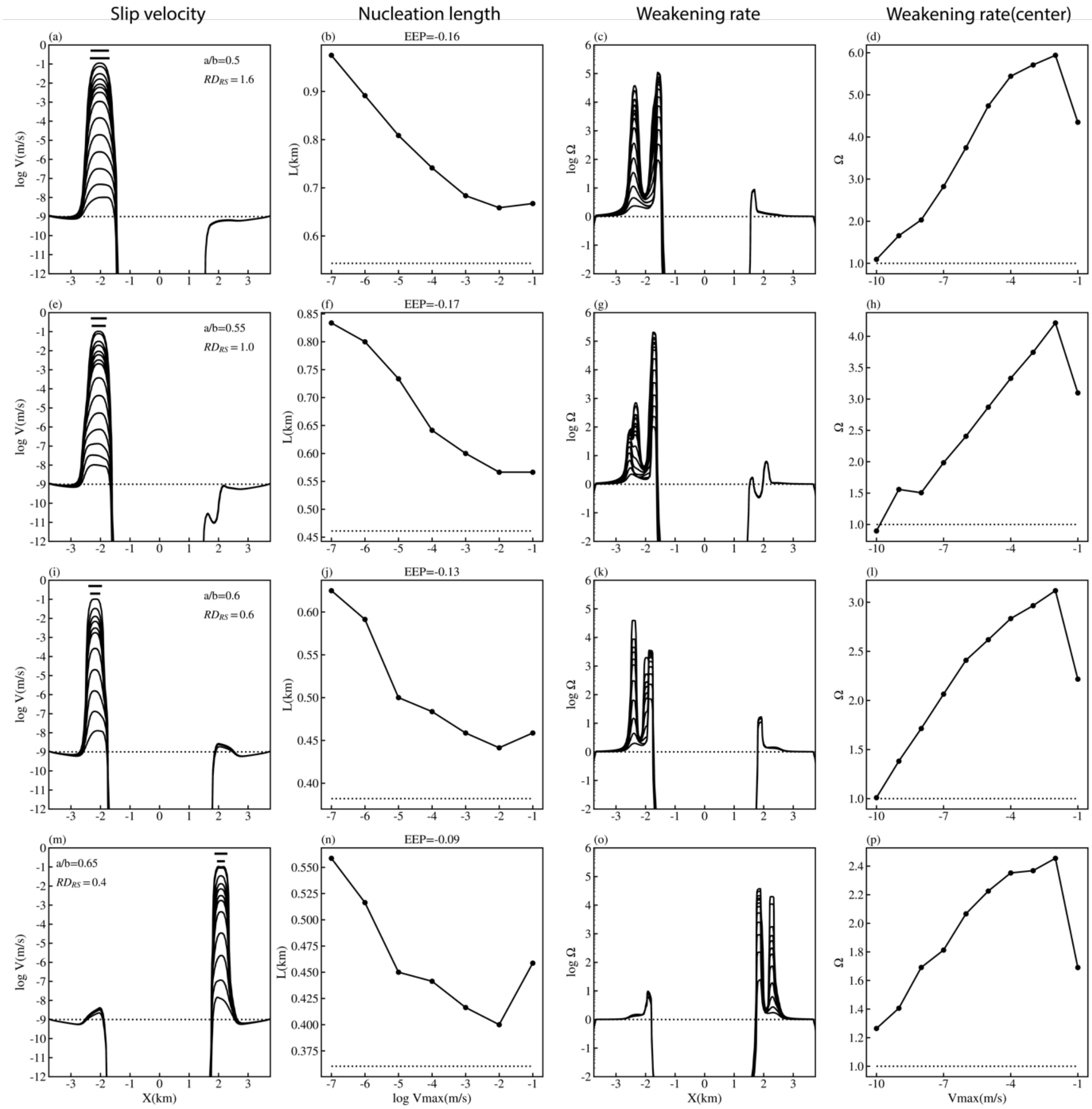

Fig. 7. Slip velocity (first column), measured nucleation length (second column), Ω (third column), and Ω in the center of the nucleation zone (fourth column) of four representative examples with unilateral ruptures, which are shown as dots surrounded by black hexagons in **Fig. 2,** respectively. In the first column, the top and bottom horizontal bars represent $2L_\infty$ and $2 * 1.3774L_b$, respectively. The dotted line in the second column represents the length of the top horizontal bar ($2L_\infty$). The dotted line in the first column is the background plate loading rate ($V_{pl} = 10^{-9}$ m/s). The dotted line in the third and fourth column refers to the constant weakening rate (Ω=1).

When a/b is in the range of 0.4 to 0.75, most cases exhibit fixed length nucleation with negative EEP values (**Fig. 7**). The weakening rate Ω within the nucleation zone keeps increasing and only decreases slightly at the final stage of nucleation. The amplitude of Ω is always lower than 10 but remains larger than 1. Thus, the yielding phase dominates the whole nucleation phase, and no expanding fracture phase occurs preceding dynamic instability. Because Ω is relatively small in these cases (only slightly larger than 1), the no-healing limit solution is not applicable and $2L_\infty$ derived for the fracture phase (top horizontal bar in the first column) still provides a good estimation of the critical nucleation length.

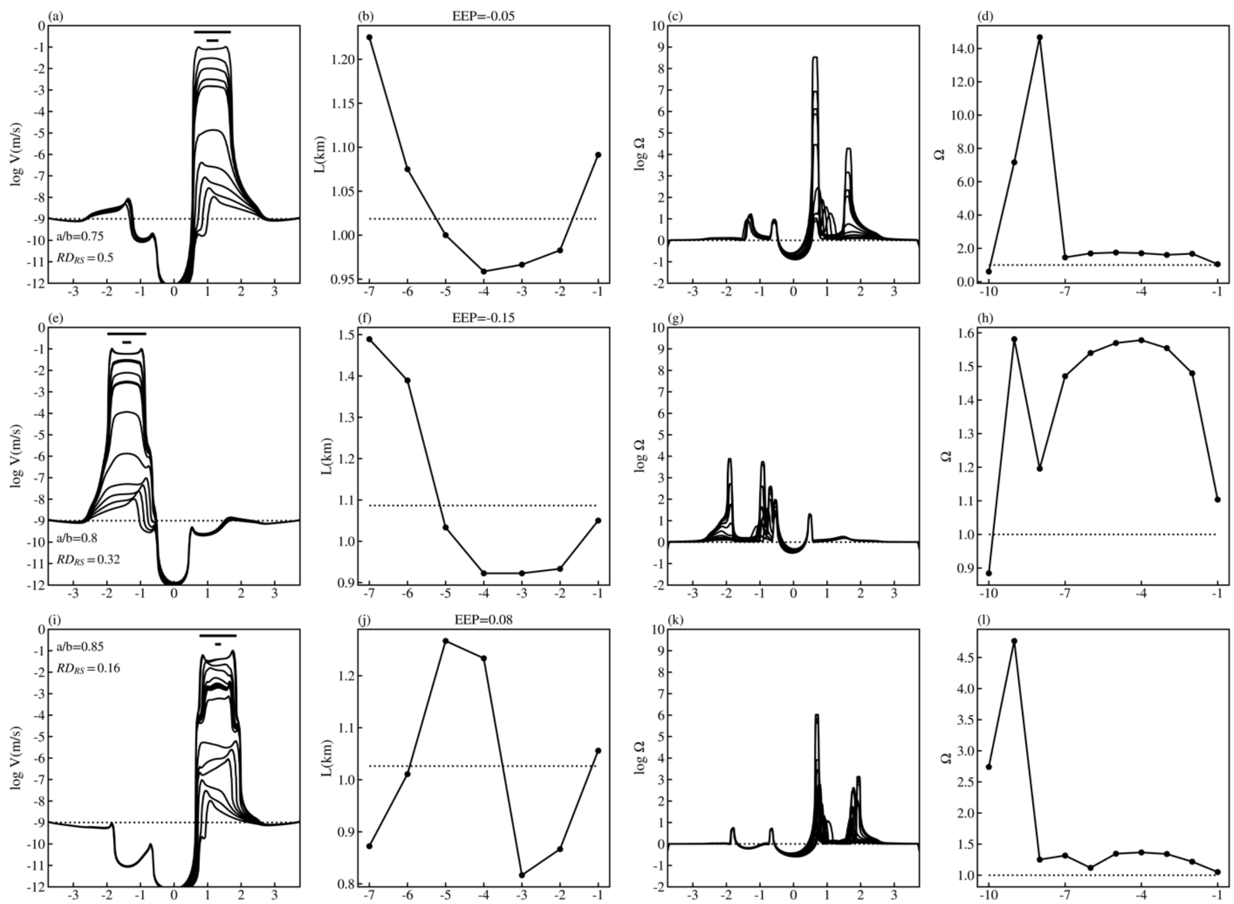

Fig. 8. Slip velocity (first column), measured nucleation length (second column), Ω (third column), and Ω in the center of the nucleation zone (fourth column) of three representative examples with complex nucleation styles, which are shown as dots surrounded by black pentagrams in **Fig. 2,** respectively. In the first column, the top and bottom horizontal bars represent $2L_\infty$ and $2 * 1.3774L_b$ respectively. The dotted line in the second column represents the length of the top horizontal bar ($2L_\infty$). The dotted line in the first column is the background plate loading rate ($V_{pl} = 10^{-9}$ m/s). The dotted line in the third and fourth column refers to the constant weakening rate (Ω=1).

But when a/b is larger (≥ 0.75), the nucleation style tends to be more complicated with unstable EEP values (either positive or negative) (**Fig. 8)**. Ω within the nucleation zone increases slightly at first and then decreases to a constant value near 1 when the maximum slip velocity exceeds about 10^{-7} m/s (**Fig. 8d, 8h and 8l**). Therefore, the fracture phase dominates the remaining nucleation phase and determines the critical nucleation length.

When the nucleation site is not in the center, a constant weakening regime with Ω near 1 results in a complex nucleation style. Taking the third case as an example (**Fig. 8i-8l**), even though the measured EEP value exceeds 0.4, it is not a typical expanding crack nucleation. Instead, the nucleation phase consists of three stages. In the first stage, the nucleation zone expands toward the left side and accelerates to a slip velocity of about 10^{-6} m/s. Then, the nucleation zone starts to expand to the right side until the slip velocity reaches about 10^{-4} m/s. During the first two acceleration stages, the nucleation zone expands unilaterally because of the asymmetric background shear stress distribution around the nucleation site. The width of the nucleation zone even exceeds the estimated critical nucleation length ($2L_{\infty}$) at a moderate slip velocity (10^{-4} m/s) prior to the nucleation threshold. Similar phenomenon also occurs in previous studies with a large a/b (e.g., **Fig. 11b** of Rubin and Ampuero, 2005). In the third stage, the nucleation zone contracts to a length smaller than $2L_{\infty}$ suddenly and then continues to expand bilaterally.

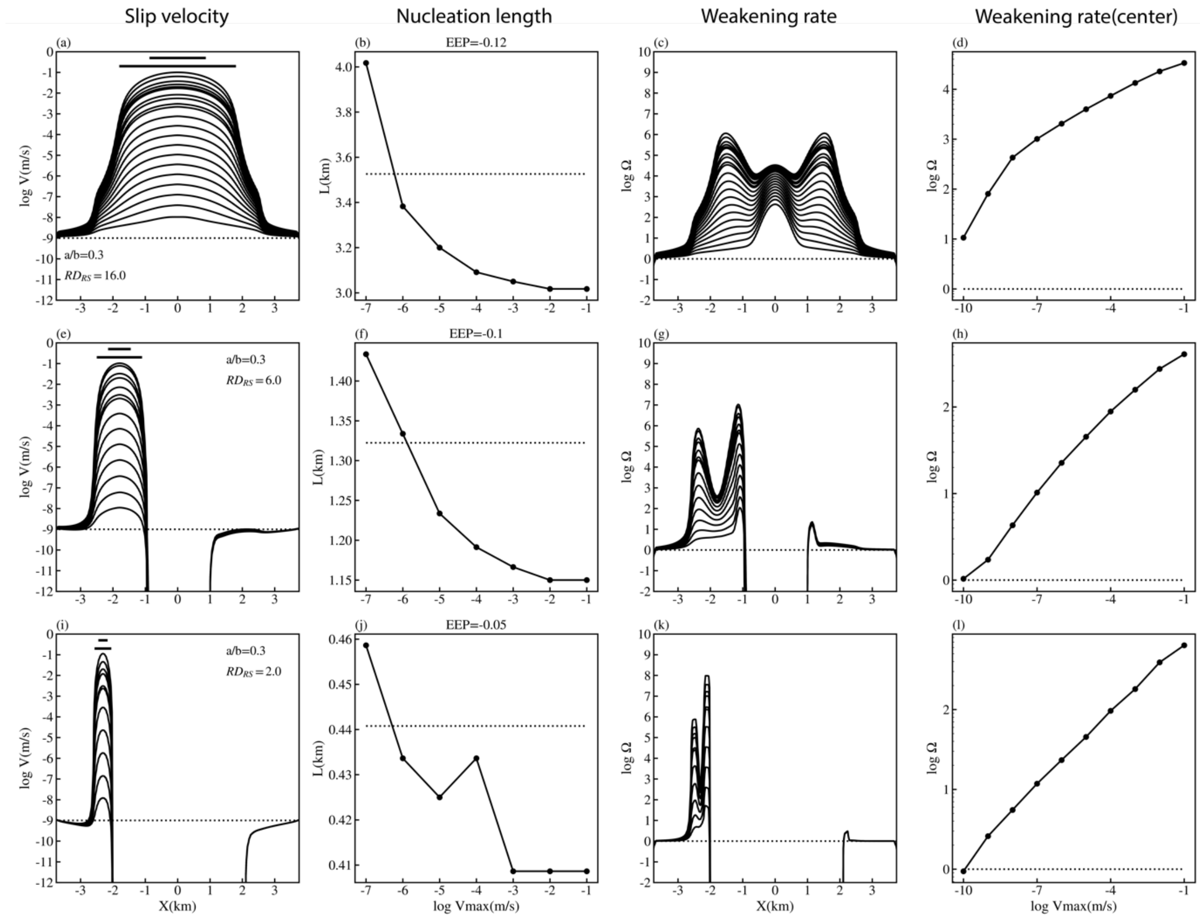

Fig. 9. Slip velocity (first column), measured nucleation length (second column), Ω (third column), and Ω in the center of the nucleation zone (fourth column) of three representative examples with no-healing limit regime, which are shown as dots surrounded by black circles in **Fig. 2,** respectively. In the first column, the top and bottom horizontal bars represent $2L_\infty$ and $2 * 1.3774L_b$ respectively. The dotted line in the second column represents the length of the bottom horizontal bar ($2 * 1.3774L_b$). The dotted line in the first column is the background plate loading rate ($V_{pl} = 10^{-9}$ m/s). The dotted line in the third and fourth column refers to the constant weakening rate (Ω=1).

4.2.3 a/b<0.3781: no-healing limit regime

When $a/b < 0.3781$, the nucleation zone keeps contracting to a fixed length, resulting in negative EEP values (**Fig. 9**). Ω increases as the slip velocity increases monotonously and no constant weakening rate can be reached before dynamic instability is triggered.

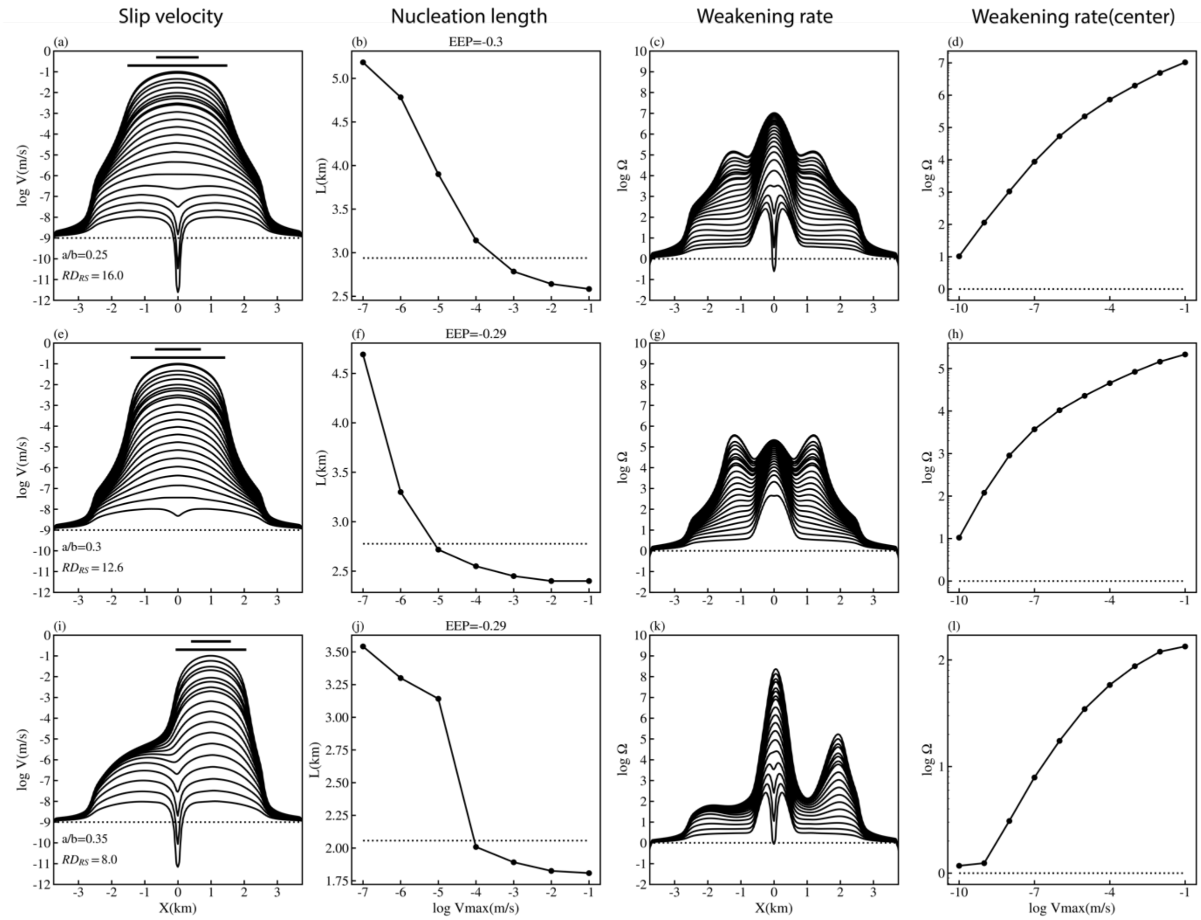

Fig. 10. Slip velocity (first column), measured nucleation length (second column), Ω (third column), and Ω in the center of the nucleation zone (fourth column) of three representative examples with an EEP of -0.3, which are shown as dots surrounded by black diamonds in **Fig. 2,** respectively. In the first column, the top and bottom horizontal bars represent $2L_\infty$ and $2 * 1.3774L_b$, respectively. The dotted line in the second column represents the length of the bottom horizontal bar ($2 * 1.3774L_b$). The dotted line in the first column is the background plate loading rate ($V_{pl} = 10^{-9}$ m/s). The dotted line in the third and fourth column refers to the constant weakening rate (Ω=1).

Moreover, around the contour line with RA=2 (or RA=4 for a/b>0.3781), which predicts the deviation of the nucleation site from the asperity center, there exists a small group of negative EEP values (black diamonds in **Fig. 2**), which correspond to twin-like nucleation styles (**Fig. 10**). A negative EEP of about -0.3 indicates that the nucleation zone contracts significantly to a small critical nucleation length. When RA~2 (or ~4 for a/b>0.3781), because both sides of the asperity accelerate at the beginning, the initial measured length of the nucleation zone (i.e., L_1) can be as large as the whole asperity width (5 km) (**Fig. 10b, 10f, 10j**). Then the nucleation zone continues to contract with two possible scenarios. In the first scenario, two early acceleration phases combine and become one single acceleration phase (**Fig. 10a and 10c**). In the second scenario, one side stops accelerating while the other side keeps growing (**Fig. 10i**).

5. Discussion

5.1 Effects of D_{RS} on nucleation style

Previously, it is commonly considered that $a/b > 0.5$ results in expanding crack nucleation. The effects of the characteristic slip distance on nucleation styles have not been explored thoroughly because it is typically used as a scale factor (e.g., Ampuero and Rubin, 2008; Fang et al., 2010; Rubin and Ampuero, 2005). However, we find that when $a/b > 0.5$, most cases have negative EEP values corresponding to a fixed length nucleation. The typical expanding crack nucleation only occurs within a narrow parameter space (a/b>0.5 and 1<RA<4). As D_{RS} decreases, an increasing a/b is needed for the generation of expanding crack nucleation.

Constrained by the computational capacity, the lowest D_{RS} explored in this study is ~0.4 mm, which is larger than the upper limit (~0.1 mm) of D_{RS} derived from laboratory experiments. However, the large gap in D_{RS} values from small-scale lab faults and large-scale natural faults suggests the existence of scale-dependence, which may be controlled by fault roughness (Scholz, 1988) and the width of the localized shear zone (Marone and Kilgore, 1993). A normalized RD_{RS} could bridge the gap of estimated D_{RS} among faults with different spatial lengths. The 5 km length asperity used in this study is an example of a natural fault subjected to a slow plate loading. I we assume that the length of natural faults lies between 1 and 100 km and D_{RS} is in the range of 0.05-0.5 m for large-scale natural faults, RD_{RS} is between 0.5 and 500, which partially overlaps with our selected parameter range of RD_{RS} (0.08-60). A similar conclusion can be found for the small-scale lab faults whose RD_{RS} is between 1 and 1000 if we assume D_{RS} is in the range of 1-100 μm for typical 0.1-1 m long lab faults. Note that using RD_{RS} larger than 60 will only lead to aseismic slip in our simulation.

5.2 Effects of nucleation site on nucleation style

For a simple uniform asperity, the typical expanding crack nucleation style only occurs with bilateral ruptures (earthquake nucleates in the center) and small enough RA (1<RA<4). Otherwise, earthquakes that nucleate at either side of the asperity cannot expand significantly even with a small constant weakening rate (~1) (**Fig. 8**). Hence, the nucleation style also depends on the specific nucleation site, which determines the consequent hypocenter and rupture style.

However, most previous numerical studies generate the nucleation phase in the center of the asperity (Ampuero and Rubin, 2008; Fang et al., 2010; Rubin and Ampuero, 2005). The nucleation sites are only allowed to vary when there are on-fault heterogeneities in the simulations, such as heterogeneous normal stress (Cattania and Segall, 2021), heterogeneous weakening rate (Lebihain et al., 2021), and non-planar fault geometry (Tal et al., 2018). Moreover, some previous studies also applied fixed boundary conditions, which artificially makes nucleation occur in the center of the asperity (Fang et al., 2010; Kaneko et al., 2016; Tal et al., 2018). In our seismic cycle model, a stable plate loading rate in our simulations permits the variation of nucleation sites, allowing seismic events to nucleate near the edge of the fault with a relatively large RA number (Barbot, 2019; Cattania, 2019). The effects of nucleation sites on nucleation styles further illuminates the necessity of studying nucleation in the context of seismic cycles (e.g., Kaneko and Ampuero, 2011; Kaneko and Lapusta, 2008). In seismic cycle models, earthquake nucleation processes naturally develop with initial conditions produced by the previous events rather than the arbitrarily selected initial conditions, which may influence the nucleation sites as well as nucleation styles.

5.3 Nucleation site (or rupture style) controlled by the RA number

To predict the nucleation site (or rupture style) within one simple uniform asperity, it is essential to estimate the critical nucleation length precisely. Nie and Barbot (2022) concluded that rupture styles can be predicted by different Ru numbers at first order. However, the Ru number is only applicable for a constant a/b, so that L_{b-a} is proportional to L_∞. The a/b used in their model is 0.75, which indicates that $R_u = \frac{8}{\pi} * RA$. In their phase diagram (**Fig. 3 in their paper**), the Ru numbers that seperate different rupture style are 3, 7.5, 18.35, 56.4, 88, which are approximately $\frac{8}{\pi}$ times of 1, 4, 8, 16, 32 recognized in our phase diagram (**Text S1 and Fig. S1-S2**). For various a/b values, the Ru number calculated from L_{b-a} is not proportional to the RA number anymore and cannot be used to separate different rupture styles. For instance, Ru number is not able to separate the SSE and regular earthquakes with different a/b ratios in one similar study (Nie and Barbot, 2021). Hence, using the RA number is more applicable for classifying rupture styles in our simulations, though there exists discrepancy (mostly <50%) between the measured and theoretical critical nucleation sizes (**Text S2 and Fig. S3**).

In our phase diagram (**Fig. S1a)**, RA=8 separates the characteristic earthquakes (including bilateral ruptures and unilateral ruptures) and other more complex rupture styles (e.g., full and partial ruptures) approximately. Based on the theoretical analysis of a half-space model, Cattania (2019) concluded that the number of earthquakes per cycle grow as

$$\alpha \sim \sqrt{\frac{W}{L_\infty}} \tag{10}$$

Where W is the length of the whole seismogenic zone. The ratio determines the seismic regimes or recurrence patterns: bimodal events for 1<α<2, characteristic (or periodic) events for α<1, and a vanishingly small fraction of system size ruptures as α>>1. Using expressions for fracture energy from RSF, the condition α=1 is satisfied by

$$\alpha \approx 0.45\sqrt{\frac{W}{L_\infty}} = 0.45\sqrt{RA} \tag{11}$$

Therefore, α=1 corresponds to RA=5±2, and RA=8 derived from our study is close to the upper limit of this range. The deviation may be caused by the usage of several fixed parameters in the theoretical analysis, such as D_{RS}=0.1 mm. It should be noted that this criterion only works for a/b>0.5 because L_∞ is derived based on fracture energy of a crack. But when a/b<0.3781 ($h^* = 2 * 1.3774L_b$), we find that RA=8 can also separate bimodal and characteristic events at first order.

5.4 Shortcomings and limitations of this study

There exists another empirical equation for the evolution of θ, or the so-called "slip law" (Ruina, 1983), where $\dot{\theta} = -\Omega ln(\Omega)$. Ampuero and Rubin (2008) compared two different evolution laws in detail and found that when $\Omega \sim 1$ (near steady state), their nucleation styles differ profoundly. For the "slip law", the nucleation zone grows as an accelerating unidirectional slip pulse rather than a crack-like expansion. In other words, the critical nucleation length could be very small as a/b approaches 1, and no analytical expression for the critical nucleation length exists. It must be borne in mind that the specific evolution of the state variable affects nucleation styles remarkably. Moreover, neither evolution law matches all the experimental data and each one can be adequate at some level. Several modifications like dependency on temperature (Barbot et al., 2023) and additional weakening mechanisms such as thermal pressurization and flash heating (Rice, 2006) have been proposed to make the predictions of RSF close to observations.

The equations derived by Rubin and Ampuero (2005) also neglect the effects of the loading rate on the critical nucleation length. For example, L_∞ is derived by assuming that slip velocity at the final stage of nucleation is much larger than the background loading rate. In our study, the constant plate loading rate is as low as 10^{-9} m/s, which naturally satisfies this condition. But faults are usually loaded with a higher slip rate (e.g., 10^{-5} m/s) in laboratory experiments, and therefore the critical nucleation length of laboratory earthquakes cannot be predicted by L_∞. Experiments carried out at different loading rates have confirmed that a larger loading rate (e.g., shorter interevent time) will produce smaller growth exponents as well as smaller critical nucleation lengths (Kaneko et al., 2016). Thus, loading rate may influence the measured EEP values as well as the specific nucleation style. Further work is needed to quantify nucleation styles in the laboratory scenarios subjected to a larger loading rate.

In this study, the idealized velocity weakening asperity has uniform frictional properties and normal stress distribution. Natural faults should have far more complex heterogeneities, which can complicate the nucleation style significantly. Lebihain et al. (2021) proposed a comprehensive framework that predicts the influence of heterogeneous weakening rate on critical nucleation length. For the extreme case, when the asperity size is between the theoretical critical nucleation length associated with average frictional properties and that of the weakest defect, small events developed within this asperity could destabilize the fault interface as a whole and generate complex dynamics of fault slip. Moreover, natural faults are more geometrically complex than a planar fault surface. Fault roughness introduced by non-planar fault surfaces complicates the nucleation phase further and can lead to non-monotonic increase of slip rate as well as multiple slip-pulses (Tal et al., 2018). Cattania and Segall (2021) studied the effects of heterogeneous normal stress caused by roughness on the nucleation phase and proposed that earthquake nucleation on rough faults is driven by the feedback between foreshocks and creep. In addition to on-fault heterogeneity, off-fault damage can also modulate the nucleation phase. It has been found that fault damage zone can significantly reduce the nucleation sizes of earthquakes in seismic cycle simulations (Thakur et al., 2020; Thakur and Huang, 2021, Mia et al., 2023).

6. Conclusion

To elucidate the prominent effects of characteristic slip distance D_{RS} on nucleation styles, we conduct fully dynamic seismic cycle simulations and analyze different kinds of nucleation styles quantitatively in the context of earthquake sequences. When D_{RS} is relatively large, a/b>0.5 leads to the expanding crack nucleation. But as D_{RS} decreases, a larger a/b (~0.75) is needed for the occurrence of expanding crack nucleation style. For a wide range of a/b (0.2-0.9) and D_{RS} (0.4mm-300mm), seismic events are more liable to nucleate as a fixed length patch rather than an expanding crack. The dominance of a fixed length nucleation indicates that the minimum size of the earthquake rupture could be estimated at the early stage of the nucleation phase.

Our simulations demonstrate that with different combinations of a/b and D_{RS}, one simple uniform asperity can generate abundant nucleation styles without complex heterogeneity. Different nucleation styles manifest different onset processes of the earthquakes and may result in distinguishable signals in seismograms. Our results shed light on the physical mechanisms underlying a variety of nucleation phases that have been observed on natural faults. Our results also suggest that we need to be cautious about choosing a specific range of D_{RS} to simulate the nucleation process as well as foreshock activities and should explore the variability of nucleation styles under more realistic conditions with complex heterogeneities and variable loading rate.

Acknowledgements

This study was supported by the National Science Foundation (Grant Award EAR-1943742).

Open research

The code employed in this research is SPEAR, an open access spectral element code in Julia, available to download in https://github.com/thehalfspace/Spear. MATLAB was used to create some figures.

Author contribution statement

Conceptualization: P. Zhai. Funding acquisition: Y. Huang. Investigation: P. Zhai, Y. Huang. Methodology: P. Zhai, Y. Huang. Supervision: Y. Huang. Validation: P. Zhai, Y. Huang Writing – original draft: P. Zhai. Writing – review & editing: P. Zhai, Y. Huang

References

Ampuero, J. P., and A. M. Rubin (2008), Earthquake nucleation on rate and state faults aging and slip laws, *J. Geophys. Res.-Solid Earth*, *113*(B1), 21, doi:10.1029/2007jb005082.

Barbot, S. (2019), Slow-slip, slow earthquakes, period-two cycles, full and partial ruptures, and deterministic chaos in a single asperity fault, *Tectonophysics*, *768*, 38, doi:10.1016/j.tecto.2019.228171.

Barbot, S. (2023), Constitutive Behavior of Rocks During the Seismic Cycle, *AGU Advances*, *4*(5), e2023AV000972, doi:10.1029/2023AV000972.

Barbot, S., N. Lapusta, and J. P. Avouac (2012), Under the hood of the earthquake machine: Toward predictive modeling of the seismic cycle, *Science*, *336*(6082), 707-710, doi:10.1126/science.1218796.

Ben-Zion, Y., and J. R. Rice (1997), Dynamic simulations of slip on a smooth fault in an elastic solid, *Journal of Geophysical Research: Solid Earth*, *102*(B8), 17771-17784, doi:10.1029/97jb01341.

Blanpied, M. L., C. J. Marone, D. A. Lockner, J. D. Byerlee, and D. P. King (1998), Quantitative measure of the variation in fault rheology due to fluid-rock interactions, *Journal of Geophysical Research: Solid Earth*, *103*(B5), 9691-9712, doi:10.1029/98JB00162.

Bouchon, M., V. Durand, D. Marsan, H. Karabulut, and J. Schmittbuhl (2013), The long precursory phase of most large interplate earthquakes, *Nature Geoscience*, *6*(4), 299-302, doi:10.1038/ngeo1770.

Campillo, M., and I. R. Ionescu (1997), Initiation of antiplane shear instability under slip dependent friction, *Journal of Geophysical Research: Solid Earth*, *102*(B9), 20363-20371, doi:10.1029/97JB01508.

Castellano, M., F. Lorez, and D. S. Kammer (2023), Nucleation of frictional slip: A yielding or a fracture process?, *Journal of the Mechanics and Physics of Solids*, *173*, 105193, doi:10.1016/j.jmps.2022.105193.

Cattania, C. (2019), Complex Earthquake Sequences On Simple Faults, *Geophys. Res. Lett.*, *46*(17-18), 10384-10393, doi:10.1029/2019gl083628.

Cattania, C., and P. Segall (2021), Precursory Slow Slip and Foreshocks on Rough Faults, *Journal of Geophysical Research: Solid Earth*, *126*(4), e2020JB020430, doi:10.1029/2020JB020430.

Chen, X., H. Yang, and M. Jin (2021), Inferring Critical Slip-Weakening Distance from Near-Fault Accelerogram of the 2014 Mw 6.2 Ludian Earthquake, *Seismological Research Letters*, doi:10.1785/0220210089.

Cocco, M., and A. Bizzarri (2002), On the slip-weakening behavior of rate- and state dependent constitutive laws, *Geophys. Res. Lett.*, *29*(11), 11-11-11-14, doi:10.1029/2001GL013999.

Day, S. M., L. A. Dalguer, N. Lapusta, and Y. Liu (2005), Comparison of finite difference and boundary integral solutions to three-dimensional spontaneous rupture, *Journal of Geophysical Research*, *110*(B12), doi:10.1029/2005jb003813.

Dieterich, J. H. (1979), Modeling of Rock Friction .1. Experimental Results and Constitutive Equations, *Journal of Geophysical Research*, *84*(Nb5), 2161-2168, doi:10.1029/JB084iB05p02161.

Dieterich, J. H. (1992), Earthquake nucleation on faults with rate-and state-dependent strength, *211*(1-4), 115-134, doi:10.1016/0040-1951(92)90055-b.

Dieterich, J. H. (2007), 4.04 - Applications of Rate- and State-Dependent Friction to Models of Fault-Slip and Earthquake Occurrence, in *Treatise on Geophysics (Second Edition)*, edited by G. Schubert, pp. 93-110, Elsevier, Oxford, doi:10.1016/B978-0-444-53802-4.00075-0.

Ellsworth, W. L., and G. C. Beroza (1995), SEISMIC EVIDENCE FOR AN EARTHQUAKE NUCLEATION PHASE, *Science*, *268*(5212), 851-855, doi:10.1126/science.268.5212.851.

Fang, Z. J., J. H. Dieterich, and G. S. Xu (2010), Effect of initial conditions and loading path on earthquake nucleation, *J. Geophys. Res.-Solid Earth*, *115*, doi:10.1029/2009jb006558.

Guatteri, M., P. Spudich, and G. C. Beroza (2001), Inferring rate and state friction parameters from a rupture model of the 1995 Hyogo-ken Nanbu (Kobe) Japan earthquake, *Journal of Geophysical Research: Solid Earth*, *106*(B11), 26511-26521, doi:10.1029/2001JB000294.

Hetland, E. A., and M. Simons (2010), Post-seismic and interseismic fault creep II: transient creep and interseismic stress shadows on megathrusts, *Geophysical Journal International*, *181*(1), 99-112, doi:10.1111/j.1365-246X.2009.04482.x.

Hetland, E. A., M. Simons, and E. M. Dunham (2010), Post-seismic and interseismic fault creep I: model description, *Geophysical Journal International*, *181*(1), 81-98, doi:10.1111/j.1365-246X.2010.04522.x.

Ide, S. (2019), Frequent observations of identical onsets of large and small earthquakes, *Nature*, *573*(7772), 112-116, doi:10.1038/s41586-019-1508-5.

Kaneko, Y., J. P. Ampuero, and N. Lapusta (2011), Spectral-element simulations of long-term fault slip: Effect of low-rigidity layers on earthquake-cycle dynamics, *J. Geophys. Res.-Solid Earth*, *116*, doi:10.1029/2011jb008395.

Kaneko, Y., and N. Lapusta (2008), Variability of earthquake nucleation in continuum models of rate-and-state faults and implications for aftershock rates, *J. Geophys. Res.-Solid Earth*, *113*(B12), doi:10.1029/2007jb005154.

Kaneko, Y., and J.-P. Ampuero (2011), A mechanism for preseismic steady rupture fronts observed in laboratory experiments, *Geophys. Res. Lett.*, *38*(21), doi:10.1029/2011GL049953.

Kaneko, Y., S. B. Nielsen, and B. M. Carpenter (2016), The onset of laboratory earthquakes explained by nucleating rupture on a rate-and-state fault, *Journal of Geophysical Research: Solid Earth*, *121*(8), 6071-6091, doi:10.1002/2016jb013143.

Kato, N. (2004), Interaction of slip on asperities: Numerical simulation of seismic cycles on a two-dimensional planar fault with nonuniform frictional property, *Journal of Geophysical Research: Solid Earth*, *109*(B12), doi:10.1029/2004jb003001.

Lapusta, N., J. R. Rice, Y. Ben-Zion, and G. T. Zheng (2000), Elastodynamic analysis for slow tectonic loading with spontaneous rupture episodes on faults with rate- and state-dependent friction, *J. Geophys. Res.-Solid Earth*, *105*(B10), 23765-23789, doi:Doi 10.1029/2000jb900250.

Latour, S., A. Schubnel, S. Nielsen, R. Madariaga, and S. Vinciguerra (2013), Characterization of nucleation during laboratory earthquakes, *Geophys. Res. Lett.*, *40*(19), 5064-5069, doi:10.1002/grl.50974.

Lebihain, M., T. Roch, M. Violay, and J.-F. Molinari (2021), Earthquake Nucleation Along Faults With Heterogeneous Weakening Rate, *Geophys. Res. Lett.*, *48*(21), e2021GL094901, doi:10.1029/2021GL094901.

Liu, Y., and J. R. Rice (2005), Aseismic slip transients emerge spontaneously in three-dimensional rate and state modeling of subduction earthquake sequences, *Journal of Geophysical Research: Solid Earth*, *110*(B8), doi:10.1029/2004JB003424.

Liu, Y., and J. R. Rice (2007), Spontaneous and triggered aseismic deformation transients in a subduction fault model, *Journal of Geophysical Research: Solid Earth*, *112*(B9), doi:10.1029/2007JB004930.

Marone, C., and B. Kilgore (1993), Scaling of the critical slip distance for seismic faulting with shear strain in fault zones, *Nature*, *362*(6421), 618-621, doi:10.1038/362618a0.

Marone, C. (1998), LABORATORY-DERIVED FRICTION LAWS AND THEIR APPLICATION TO SEISMIC FAULTING, *Annual Review of Earth and Planetary Sciences*, *26*(1), 643-696, doi:10.1146/annurev.earth.26.1.643.

McGuire, J. J., M. S. Boettcher, and T. H. Jordan (2005), Foreshock sequences and short-term earthquake predictability on East Pacific Rise transform faults, *Nature*, *434*(7032), 457-461, doi:10.1038/nature03377.

McLaskey, G. C., and B. D. Kilgore (2013), Foreshocks during the nucleation of stick-slip instability, *Journal of Geophysical Research: Solid Earth*, *118*(6), 2982-2997, doi:10.1002/jgrb.50232.

McLaskey, G. C. (2019), Earthquake Initiation From Laboratory Observations and Implications for Foreshocks, *Journal of Geophysical Research: Solid Earth*, *124*(12), 12882-12904, doi:10.1029/2019jb018363.

Mia, M. S., M. Abdelmeguid, and A. E. Elbanna (2023), The spectrum of fault slip in elastoplastic fault zones, *Earth and Planetary Science Letters*, *619*, 118310, doi:10.1016/j.epsl.2023.118310.

Nie, S., and S. Barbot (2021), Seismogenic and tremorgenic slow slip near the stability transition of frictional sliding, *Earth and Planetary Science Letters*, *569*, 117037, doi:10.1016/j.epsl.2021.117037.

Nie, S., and S. Barbot (2022), Rupture styles linked to recurrence patterns in seismic cycles with a compliant fault zone, *Earth and Planetary Science Letters*, *591*, 117593, doi:10.1016/j.epsl.2022.117593.

Ohnaka, M., and L.-f. Shen (1999), Scaling of the shear rupture process from nucleation to dynamic propagation: Implications of geometric irregularity of the rupturing surfaces, *Journal of Geophysical Research: Solid Earth*, *104*(B1), 817-844, doi:10.1029/1998JB900007.

Reinen, L. A., T. E. Tullis, and J. D. Weeks (1992), Two-mechanism model for frictional sliding of serpentinite, *Geophys. Res. Lett.*, *19*(15), 1535-1538, doi:10.1029/92GL01388.

Rice, J. R. (1993), SPATIOTEMPORAL COMPLEXITY OF SLIP ON A FAULT, *J. Geophys. Res.-Solid Earth*, *98*(B6), 9885-9907, doi:10.1029/93jb00191.

Rice, J. R., and Y. Ben-Zion (1996), Slip complexity in earthquake fault models, *Proceedings of the National Academy of Sciences*, *93*(9), 3811-3818, doi:doi:10.1073/pnas.93.9.3811.

Rice, J. R., N. Lapusta, and K. Ranjith (2001), Rate and state dependent friction and the stability of sliding between elastically deformable solids, *Journal of the Mechanics and Physics of Solids*, *49*(9), 1865-1898, doi:10.1016/S0022-5096(01)00042-4.

Rice, J. R. (2006), Heating and weakening of faults during earthquake slip, *Journal of Geophysical Research: Solid Earth*, *111*(B5), doi:10.1029/2005jb004006.

Rubin, A. M. (2008), Episodic slow slip events and rate-and-state friction, *Journal of Geophysical Research: Solid Earth*, *113*(B11), doi:https:10.1029/2008JB005642.

Rubin, A. M., and J. P. Ampuero (2005), Earthquake nucleation on (aging) rate and state faults, *Journal of Geophysical Research: Solid Earth*, *110*(B11), doi:10.1029/2005JB003686.

Ruina, A. (1983), Slip instability and state variable friction laws, *Journal of Geophysical Research*, *88*(NB12), 359-370, doi:10.1029/JB088iB12p10359.

Scholz, C. H. (1988), The critical slip distance for seismic faulting, *Nature*, *336*(6201), 761-763, doi:10.1038/336761a0.

Scholz, C. H. (1998), Earthquakes and friction laws, *Nature*, *391*(6662), 37-42, doi:10.1038/34097.

Tal, Y., B. H. Hager, and J. P. Ampuero (2018), The Effects of Fault Roughness on the Earthquake Nucleation Process, *Journal of Geophysical Research: Solid Earth*, *123*(1), 437-456, doi:10.1002/2017JB014746.

Tape, C., S. Holtkamp, V. Silwal, J. Hawthorne, Y. Kaneko, J. P. Ampuero, C. Ji, N. Ruppert, K. Smith, and M. E. West (2018), Earthquake nucleation and fault slip complexity in the lower crust of central Alaska, *Nature Geoscience*, *11*(7), 536-541, doi:10.1038/s41561-018-0144-2.

Thakur, P., and Y. H. Huang (2021), Influence of Fault Zone Maturity on Fully Dynamic Earthquake Cycles, *Geophys. Res. Lett.*, *48*(17), doi:10.1029/2021GL094679.

Thakur, P., Y. H. Huang, and Y. Kaneko (2020), Effects of Low-Velocity Fault Damage Zones on Long-Term Earthquake Behaviors on Mature Strike-Slip Faults, *J. Geophys. Res.-Solid Earth*, *125*(8), doi:10.1029/2020JB019587.

Tse, S. T., and J. R. Rice (1986), CRUSTAL EARTHQUAKE INSTABILITY IN RELATION TO THE DEPTH VARIATION OF FRICTIONAL SLIP PROPERTIES, *Journal of Geophysical Research-Solid Earth and Planets*, *91*(B9), 9452-9472, doi:10.1029/JB091iB09p09452.

Uenishi, K., and J. R. Rice (2003), Universal nucleation length for slip-weakening rupture instability under nonuniform fault loading, *J. Geophys. Res.-Solid Earth*, *108*(B1), doi:10.1029/2001jb001681.

Werner, M. J., and A. M. Rubin (2013), Mechanical Erosion of the Seismogenic Zone by Creep from below on Rate-and-State Faults, edited, pp. T53E-06.

Wu, Y., and X. Chen (2014), The scale-dependent slip pattern for a uniform fault model obeying the rate- and state-dependent friction law, *Journal of Geophysical Research: Solid Earth*, *119*(6), 4890-4906, doi:10.1002/2013JB010779.

Supplemental information

Text S1.

Recognition of Different Rupture Styles

With the selected parameters of a/b and D_{RS}, we produce all kinds of rupture styles, including steady sliding, slow slip events, bilateral and unilateral ruptures, full and partial ruptures, crack-like ruptures and combination of pulse and crack ruptures with small aftershocks. Each rupture style occurs within a specific range of RA numbers. In other words, distinct rupture styles can be predicted by contours of RA number at first order **(Fig. S1a).**

For cases with a/b > 0.3781, the transitions from aseismic slip to symmetric-bilateral ruptures, to unsymmetric bilateral and unilateral ruptures, to full and partial ruptures, and to crack-like ruptures and combination of pulse and crack ruptures with aftershocks occur at RA = 1, 4, 8, 16, 32, respectively. For cases with a/b < 0.3781, the boundaries of different rupture styles are different, and transitions occur at RA = 0.5, 2, 8, 12, 18.

It should be noted that for a/b<0.3781 and RA<1, regular seismic events (with peak slip velocity > 0.1 m/s) still happen, which conflicts with the concept that when the theoretical critical nucleation length is larger than the asperity size, no seismic event can occur. The reason may be that the asperity has a strong weakening property when a/b is relatively small. During the slow (or sluggish) nucleation process with a small RA number (~1), slip is prone to penetrate the neighboring barrier (i.e. velocity strengthening zone). Therefore, regular seismic events (with peak slip velocity > 0.1 m/s) can still happen when RA is smaller than 1, which are not explored further in this study.

We outline the specific definition of each term below:

Aseismic slip (Fig. S1b): steady sliding or slow slip events with maximum slip velocity <0.1 m/s (nucleation threshold).

Characteristic (Fig. S1c-S1d): Full ruptures with regular recurrence interval. We use $df = 2|S - Sc|/W$ to describe the deviation of nucleation site S from the center of the velocity-weakening asperity Sc.

Symmetric bilateral: hypocenter is nearly in the center of the asperity (0<df<0.2)

Unsymmetric bilateral: (0.2<df<0.6)

Unilateral: (0.6<df<1)

Full and partial ruptures (Fig. S1e): A combination of full and partial ruptures. Here the partial rupture means the rupture length exceeds 2.5 km (half-length of asperity) but not a full rupture.
Crack-like ruptures with aftershocks (Fig. S1f): Here the aftershocks mean those seismic events with rupture length smaller than 2.5 km.
Combination of pulse and crack with aftershocks (Fig. S1g): Occurrence of multiple slip velocity pulses accompanied by crack and aftershocks.

A further comparison of crack-like rupture and combination of pulse and crack rupture is displayed by **Fig. S2**.

Text S2.

Discrepancy between the measured critical nucleation length and the theoretical estimation

Those contours in **Fig. 2 and Fig. S1a** are plotted using the theoretical critical nucleation length derived by Rubin and Ampuero (2005). But the ability that RA number can predict rupture styles significantly relies on the accuracy of the theoretical estimation. There exists a certain amount of discrepancy between the measured critical nucleation length and the theoretical estimation (**Fig. S3**).

Here, we define the $L_{0.1}$ (i.e. L_7: the measured width of slip velocity distribution over 10^{-2} m/s when the maximum slip velocity just exceeds the selected nucleation threshold: 0.1 m/s) as the measured critical nucleation length. $L_{0.1}$ is only an approximation of the practical nucleation length based on the slip velocity distribution. Another way to obtain the critical nucleation length is to measure the peak-to-peak distance of the stressing rate distribution (or Ω) (Fang et al. 2010; Rubin and Ampuero, 2005).

Obviously, the theoretical equation derived from fracture energy balance only works well when a/b is larger than 0.5 as suggested by (Rubin and Ampuero, 2005). When a/b is around 0.4, $L_{0.1}$ tends to be larger than the corresponding theoretical value and the largest deviation exceeds half of the theoretical estimation h^* (>50%). The reason is that, when a/b is smaller than 0.5, a yielding phase scaled by L_b is prone to dominate the whole nucleation process without a second fracture phase scaled by L_∞. In this case, the half-length of the critical nucleation zone should be larger than L_∞ and approach the no-healing limit solution $1.3774L_b$. In addition, the measured critical nucleation length of the case in **Fig. 6** is also smaller than the theoretical estimation ($2L_\infty$) even when a/b>0.5 because it is the small-scale yielding phase rather than the fracture phase that determines the critical nucleation length.

Even though the typical expanding crack nucleation style is not common for other complex rupture styles with RA>4, L_∞ derived from the energy-based equation can still predict the critical nucleation length well for those cases with a/b>0.5 and a wide range of RD_{RS}. The reason may be that the weakening rate within the nucleation zone has already become small enough (<10) preceding the dynamic instability (**Fig. 7d, 7h, 7l, 7p**). On the other hand, $1.3774L_b$ works well in most cases with a/b<0.3781.

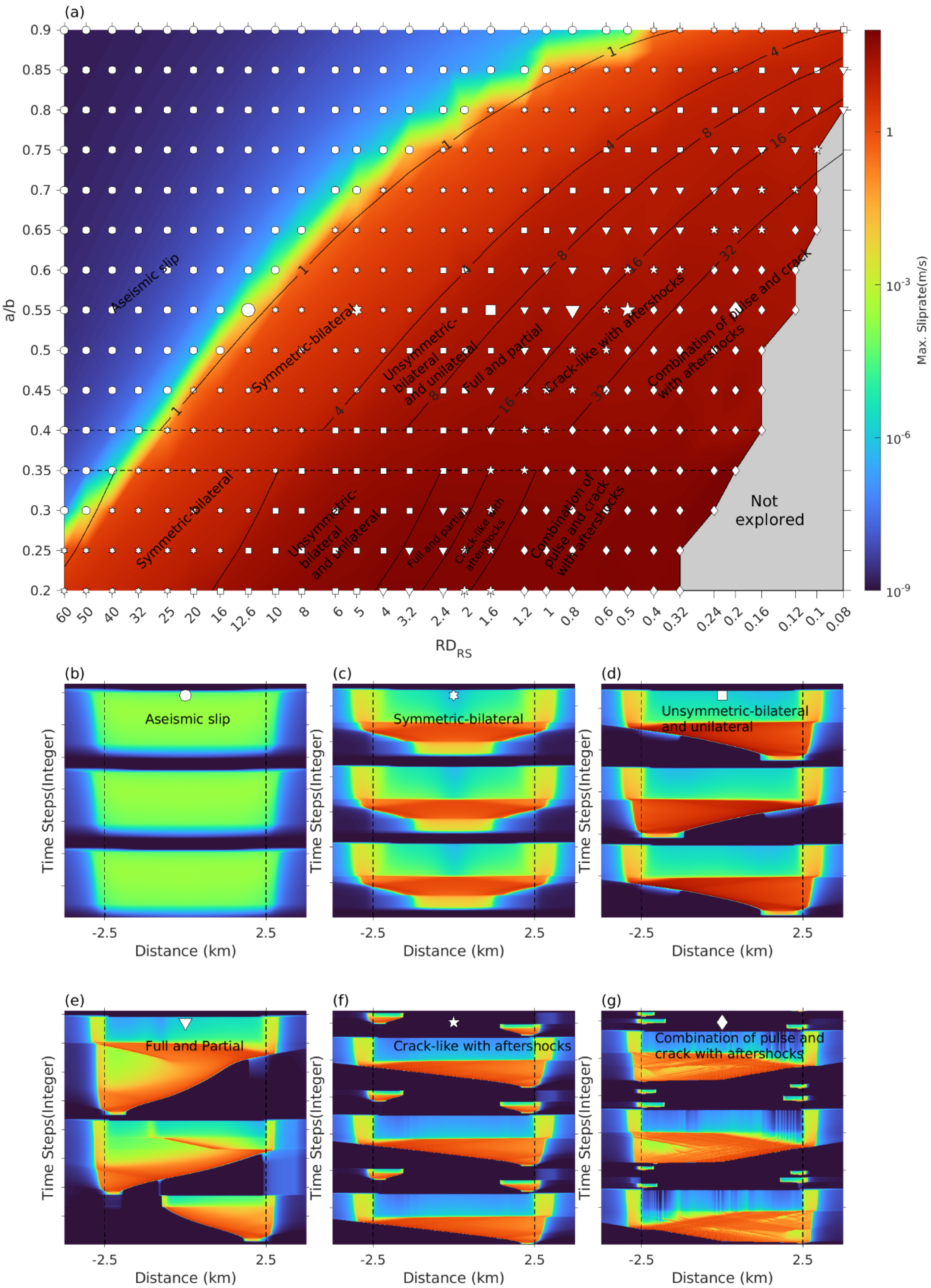

(a)
Aseismic slip
Symmetric-bilateral
Unsymmetric-bilateral and unilateral
Full and partial
Crack-like with aftershocks
Combination of pulse and crack with aftershocks
Not explored
a/b
RD_RS
Max. Sliprate(m/s)
(b)
Aseismic slip
(c)
Symmetric-bilateral
(d)
Unsymmetric-bilateral and unilateral
(e)
Full and Partial
(f)
Crack-like with aftershocks
(g)
Combination of pulse and crack with aftershocks
Time Steps(Integer)
Distance (km)

880

Fig. S1. (a) Maximum slip velocity in seismic cycles under variable normalized characteristic slip distance (RD_{RS}) and a/b. Contours are the RA numbers of the models. The symbols represent different rupture styles. **(b-g)** Slip velocity evolution of different rupture styles. The x- and y-axes represent down-dip distance on the fault and non-constant time steps, respectively.

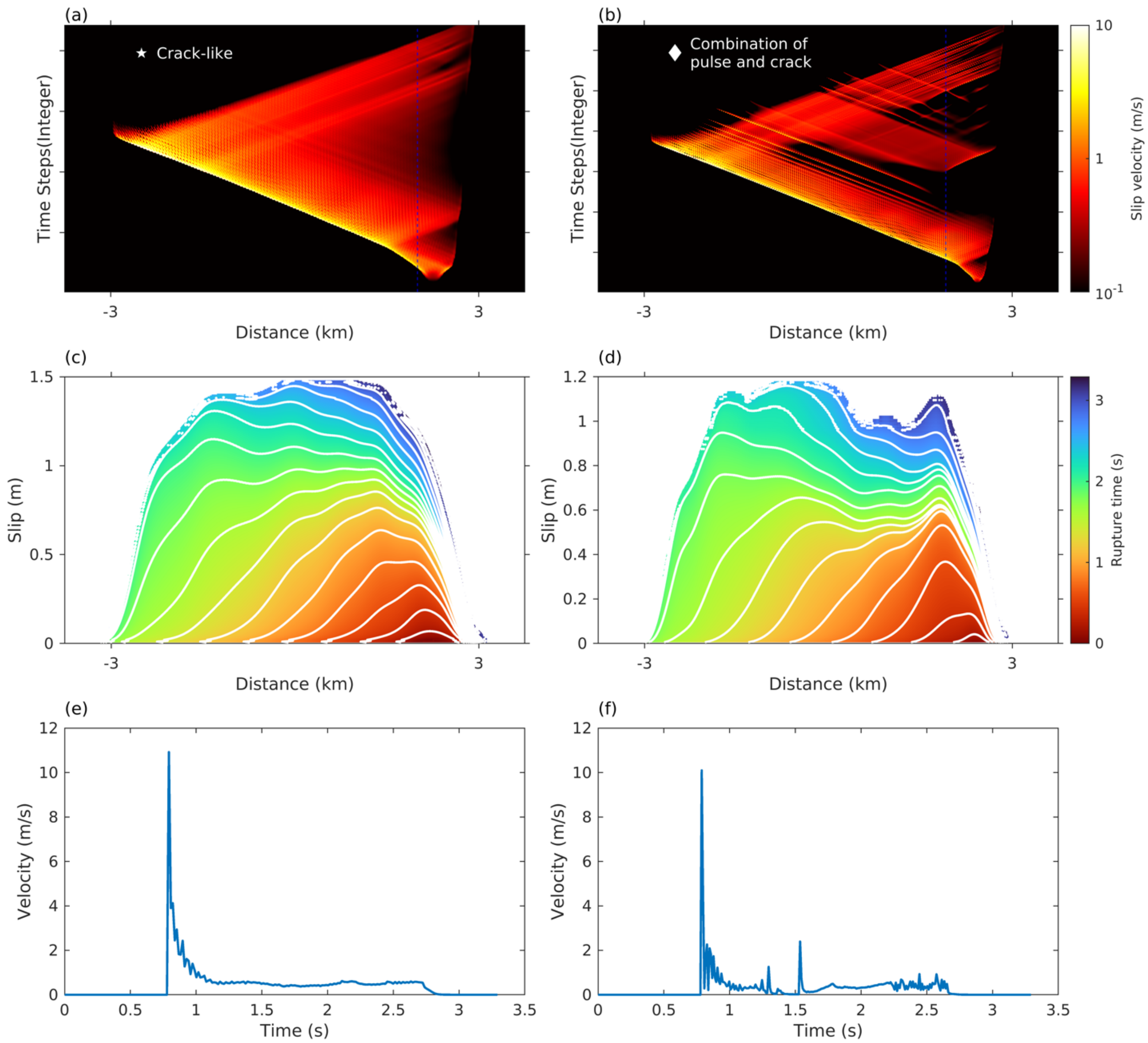

Fig. S2 A detailed comparison between crack-like and combination of pulse and crack ruptures. **(a-b)** Slip velocity versus time steps. **(c-d)** Rupture history with 0.2-second interval contour. **(e-f)** Source-time function with the sampling locations shown as blue dash lines in panel (a) and (c) respectively.

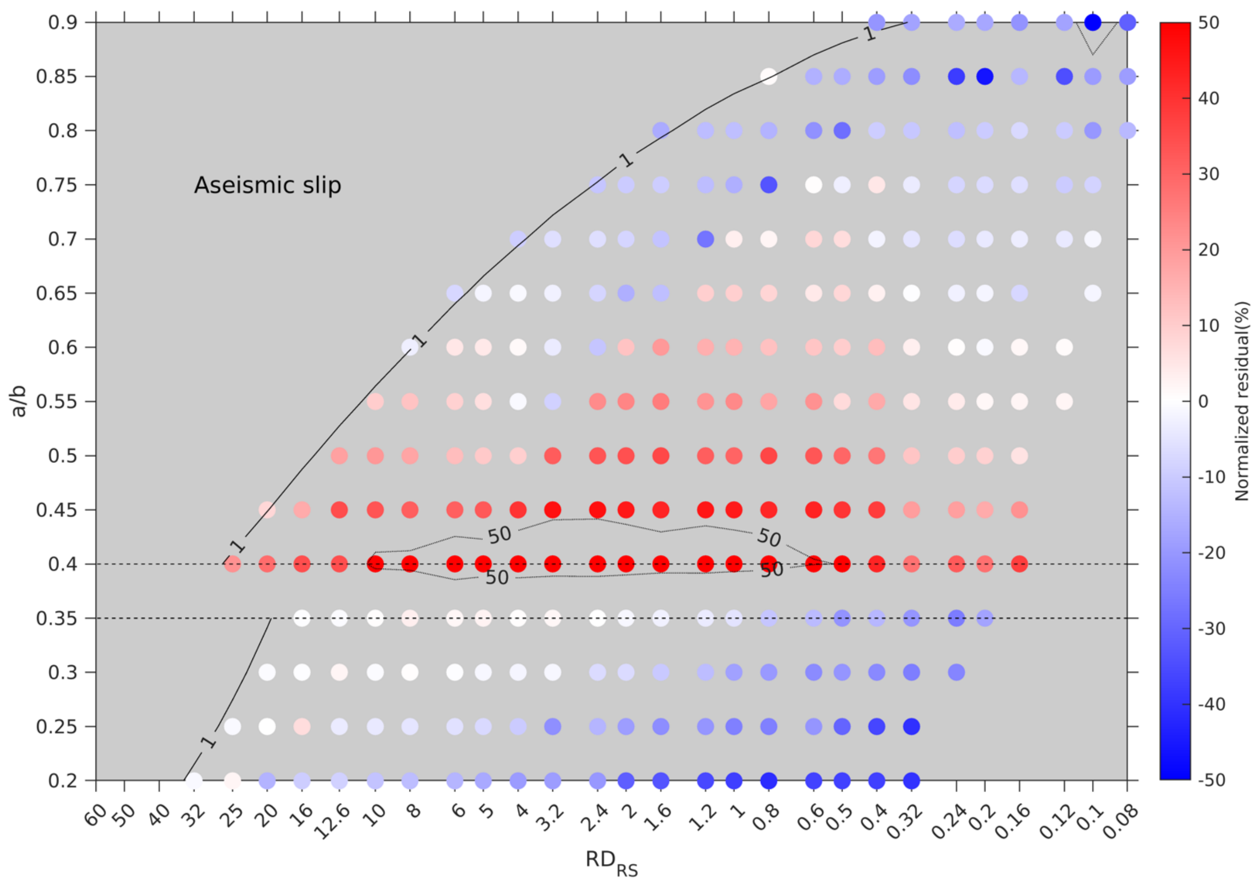

Fig. S3 Normalized residual ($\frac{L_{0.1}-h^*}{h^*}$) between the measured $L_{0.1}$ and the theoretical critical nucleation length h^* in percentage. The black contour corresponds to RA=1, which separates aseismic slip and regular seismic events (with maximum slip velocity > 0.1 m/s). Black dotted lines are contours with 50% normalized residual.

References for the supplemental information

Fang, Z. J., J. H. Dieterich, and G. S. Xu (2010), Effect of initial conditions and loading path on earthquake nucleation, *J. Geophys. Res.-Solid Earth*, *115*, doi:10.1029/2009jb006558.

Rubin, A. M., and J. P. Ampuero (2005), Earthquake nucleation on (aging) rate and state faults, *Journal of Geophysical Research: Solid Earth*, *110*(B11), doi:10.1029/2005JB003686.